# Molecular-Level Electron Transfer and Excited State Assemblies on Surfaces of Metal Oxides and Glass

**Thomas J. Meyer,* Gerald J. Meyer, Brian W. Pfennig, Jon R. Schoonover, Cliff J. Timpson, Jennifer F. Wall, Claus Kobusch, Xiaohong Chen, Brian M. Peek, Craig G. Wall, Wei Ou, Bruce W. Erickson, and Carlo A. Bignozzi†**

Department of Chemistry, The University of North Carolina, Chapel Hill, North Carolina 27599-3290, and Dipartimento di Chimia, Universita di Ferrara, Via L. Borsai N. 46, 44100 Ferrara, Italy

*Received July 23, 1993**

A general procedure is described for the attachment to antimony-doped tin dioxide ($SnO_2$:Sb), tin-doped indium oxide ($In_2O_3$:Sn), or glass surfaces of molecules with known electron transfer or excited state properties, e.g. [Ru(bpy)$_2$(4,4′-(CO$_2$H)$_2$bpy)](PF$_6$)$_2$ (bpy = 2,2′-bipyridine, 4,4′-(CO$_2$H)$_2$bpy = 4,4′-dicarboxy-2,2′-bipyridine), based on the interaction between surface hydroxyls and carboxylic acid groups. Integrations of cyclic voltammetric waveforms on the metal oxide electrodes give maximum surface coverages of $\Gamma \sim 1 \times 10^{-10}$ mol/cm$^2$ for the ruthenium complex, which corresponds to a monolayer coverage. Atomic force microscope (AFM) measurements reveal that the metal oxide surfaces are highly roughened with root mean square roughnesses in the range 4–6.5 nm for tin oxide. The smaller organics, *N*-methyl-*N*-viologenpropanoic acid bis(hexafluorophosphate), [MV-CO$_2$H](PF$_6$)$_2$, and 10*H*-phenothiazine-10-propanoic acid, PTZ-CO$_2$H, display similar surface coverages. Resonance Raman measurements on surfaces containing the ruthenium complex imply that attachment to $SnO_2$, $In_2O_3$, and $TiO_2$ is via an ester bond. For $SiO_2$, two modes of binding are suggested, a majority by a chelating carboxylato link and a minority by ester formation. Binding constants for surface attachment were measured in $CH_2Cl_2$ at 298 K by equilibration, which gave $K = 8 \times 10^4$ M$^{-1}$ on both $SnO_2$:Sb and $In_2O_3$:Sn. Surface molecular assemblies have been prepared containing [Ru(bpy)$_2$(4,4′-(CO$_2$H)$_2$bpy)](PF$_6$)$_2$ and [Os(bpy)$_2$(4,4′-(CO$_2$H)$_2$ bpy)](PF$_6$)$_2$, [MV-CO$_2$H](PF$_6$)$_2$, and PTZ-CO$_2$H. In these assemblies, separate waves are observed for the different redox couples at potentials near those found for surfaces containing only a single component. Emission decay of the metal-to-ligand charge transfer (MLCT) excited state of [Ru(bpy)$_2$(4,4′-(CO$_2$H)$_2$bpy)](PF$_6$)$_2$ attached to the glass backings of metal oxide electrodes or to glass slides was found to be nonexponential with average lifetimes ($\langle\tau\rangle$) from < 5 to 600 ns with $CH_2Cl_2$ in the external solution. $\langle\tau\rangle$ increases as surface coverage decreases. There is evidence for excited state–ground state interactions by a red-shift in the emission maximum as surface coverage increases. Emission decay remains nonexponential even on surfaces that are lightly covered. Emission is nearly completely quenched on the semiconductor surfaces, with $\langle\tau\rangle < 5$ ns. The bound Ru(II) emitters on glass were quenched by electron or energy transfer to the coattached quenchers [MV-CO$_2$H](PF$_6$)$_2$, PTZ-CO$_2$H, or [Os(bpy)$_2$(4,4′-(CO$_2$H)$_2$-bpy)](PF$_6$)$_2$, suggesting that lateral electron and energy transfer can occur across the surface. Surface lifetime quenching also occurred in the presence of added 10-methyl-10-phenothiazene in the external $CH_2Cl_2$ solution. The kinetics of lifetime quenching did not follow Stern–Volmer kinetics but could be fit to a model in which there are both quenchable and unquenchable sites on the same surface.

## Introduction

The formation and characterization of structurally well-defined arrays of redox or photoactive molecules on insulating or semiconductor substrates is potentially an important element in the design of molecular-level devices. Among the approaches used to form these arrays have been Langmuir–Blodgett films,[1] the formation of surface bonds on gold,[2] or pyridine bonds on platinum or silver.[3] Another is the "self-assembly" of carboxylic acid-containing molecules on metal oxides, presumably through ester bond formation between the carboxylic acid and surface hydroxyl groups. This approach has been used to sensitize wide band gap semiconductors with carboxylic acid derivatives of polypyridyl complexes,[4] organic dyes,[5] porphyrins,[6] and aromatic hydrocarbons.[7]

* To whom correspondence should be addressed at the University of North Carolina.

† Universita di Ferrara.

* Abstract published in *Advance ACS Abstracts,* June 15, 1994.

(1) (a) Fujihara, M.; Nishiyama, K.; Aoki, K. *Thin Solid Films* **1988**, *160*, 317. (b) Fujihara, M.; Yamada, H. *Thin Solid Films* **1988**, *160*, 125. (c) Kondo, T.; Yamada, H.; Nishiyama, K.; Suga, K.; Fujihara, M. *Thin Solid Films* **1989**, *179*, 463. (d) Fujihara, M.; Sakomura, M. *Thin Solid Films* **1989**, *179*, 471. (e) Fujihara, M.; Sakomura, M. *Thin Solid Films* **1989**, *180*, 43.

(2) (a) Chidsey, C. E. D.; Loiacono, D. N. *Langmuir* **1990**, *6*, 682 and references therein. (b) Nuzzo, R. G.; Dubois, L. H.; Allara, D. L. *J. Am. Chem. Soc.* **1990**, *112*, 558. (c) Bain, C. D.; Troughton, E. B.; Tao, Y.-T.; Evall, J.; Whitesides, G. M.; Nuzzo, R. G. *J. Am. Chem. Soc.* **1989**, *111*, 321. (d) Troughton, E. B.; Bain, C. B.; Whitesides, G. M.; Nuzzo, R. G.; Allara, D. L.; Porter, M. D. *Langmuir* **1988**, *4*, 365. (e) Bain, C. D.; Whitesides, G. M. *Science* **1988**, *240*, 62. (f) Harris, A. L.; Chidsey, C. E. D.; Levinos, N. J.; Loiacono, D. N. *Chem. Phys. Lett.* **1987**, *141*, 350. (g) Dubois, L. H.; Zegarski, B. R.; Nuzzo, R. G. *Proc. Natl. Acad. Sci. U.S.A.* **1987**, *84*, 4739.

(3) (a) Schlotter, N. E.; Porter, M. D.; Bright, T. B.; Allara, D. L. *Chem. Phys. Lett.* **1986**, *132*, 93. (b) Columbia, M. R.; Crabtree, A. M.; Thiel, P. A. *J. Am. Chem. Soc.* **1992**, *114*, 1231. (c) Acevedo, D.; Abruña, H. D. Personal communication.

(4) (a) Anderson, S.; Constable, E. C.; Dare-Edwards, M. P.; Goodenough, J. B.; Hamnett, A.; Seddon, K. R.; Wright, R. D *Nature* **1979**, *280*, 571. (b) Goodenough, J. B.; Hamnett, A.; Dare-Edwards, M. P.; Campet, G.; Wright, R. D. *Surf. Sci.* **1980**, *101*, 531. (c) Dare-Edwards, M. P.; Goodenough, J. B.; Hamnett, A.; Seddon, K. R.; Wright, R. D. *Faraday Discuss. Chem. Soc.* **1980**, *70*, 285. (d) Vlachopoulos, N.; Liska, P.; Augustynski, T.; Grätzel, M. *J. Am. Chem. Soc.* **1988**, *110*, 1216. (e) Desilvestro, J.; Grätzel, M.; Kavan, L.; Moser, J. *J. Am. Chem. Soc.* **1985**, *107*, 2988. (f) Liska, P.; Vlachopoulos, N.; Nazeeruddin, M. K.; Comte, P.; Grätzel, M. *J. Am. Chem. Soc.* **1988**, *110*, 3686. (g) Furlong, D. N.; Wells, D.; Sasse, W. H. F. *J. Phys. Chem.* **1986**, *90*, 1107. (h) Takemura, H.; Saji, T.; Fujihara, M.; Aoyagui, S.; Hashimoto, K.; Sakata, T. *Chem. Phys. Lett.* **1985**, *122*, 496. (i) Hashimoto, K.; Hiramoto, M.; Sakata, T.; Muraki, H.; Takemura, H.; Fujihara, M. *J. Phys. Chem.* **1987**, *97*, 6198. (j) Amadelli, R.; Argazzi, R.; Bignozzi, C. A.; Scandola, F. *J. Am. Chem. Soc.* **1990**, *112*, 7099. (k) Christ, Jr., C. C.; Yu, J.; Zhao, X.; Palmore, G. T. R.; Wrighton, M. S. *Inorg. Chem.* **1992**, *31*, 4439.

0020-1669/94/1333-3952$04.50/0 

We are exploring interfacial chemistry based on carboxylic acid–surface interactions with the goal of preparing complex, molecular-level assemblies having well-defined redox or excited state properties. We describe here the surface attachment and photophysical properties of polypyridyl complexes of Ru(II), carboxylic acid derivatives of phenothiazine or methyl viologen, and mixtures of the three on metal oxide surfaces or glass and the application of resonance Raman spectroscopy to the elucidation of surface binding.

## Experimental Section

**Materials.** The solvents $CH_2Cl_2$ (Mallinckrodt; 99.9%), $CH_3CN$ (Baxter; B&J High Purity), $CH_3OH$ (Baxter; B&J High Purity), $C_2H_5OH$ (Aaper Alcohol and Chemical Co.; Absolute), cyclohexane (Aldrich; 99.9+ %) and carbon tetrachloride (Mallinckrodt; 99.9%) were used as received. The acids and salts $H_2SO_4$ (Aldrich; 99.99%), $Na_2SO_4$ (Aldrich; 99%), and $HPF_6$ (Aldrich; 60 wt %), as well as dicyclohexylcarbodiimide (DCC) (Aldrich; 99%) were also used as received. $[N(n\text{-}C_4H_9)_4](PF_6)$ (Aldrich; 99.99%) was recrystallized from ethanol prior to use. Prefabricated antimony-doped tin oxide (ATO; $SnO_2$:Sb) and tin-doped indium oxide (ITO; $In_2O_3$:Sn) coated glass slides were purchased from Delta Tech. Ltd.; Stillwater, MN. In general, the slides were nominally 1–3 mm thick on a soda lime glass subtrate with the optically transparent conductive film (ATO or ITO) deposited on one side of the insulating glass. The ATO slides (50 mm × 75 mm) were cut into ~1-cm strips with either a carbide blade circular saw (Wilt Ind. Inc.; Lake Pleasant NY) or by first scoring the glass side with a diamond tipped stylus and then cleaving along the score with pressure. The ITO slides were available precut by the manufacturer to fit standard cuvettes (7 mm × 50 mm).

**Syntheses. *N*-Methyl-*N*-viologenpropanoic Acid Bis(hexafluorophosphate).** A solution containing 3.2 g of N-methyl-4,4′-bipyridine and 3.85 g of 3-bromopropionic acid in 40 mL of dimethylformamide (DMF) was stirred for 5 days during which time a precipitate formed. The solid was dissolved in 7 mL of $H_2O$ and precipitated with saturated $[NH_4](PF_6)$. Recrystallization from 1:1 (v:v) MeOH/water with a trace of $[NH_4](PF_6)$ added, yielded 0.81 g of the pure salt, *N*-methyl-*N*-viologenpropionic acid bis(hexafluorophosphate) in 15% yield. UV ($CH_3CN$): λ (ε) 260 nm (20 100 $M^{-1}$ $cm^{-1}$). $^1H$ NMR (200 MHz, acetone-$d_6$): δ 3.39 (t, $J$ = 6.32 Hz, 2H, α-$CH_2$), 4.74 (s, 3H, $CH_3$), 5.21 (t, $J$ = 6.62 Hz, 2H, β-$CH_2$), 8.82 (d, $J$ = 6.62 Hz, 2H, aromatic), 8.84 (d, $J$ = 6.96 Hz, 2H, aromatic), 9.36 (d, $J$ = 6.84 Hz, 2H, aromatic), 9.49 (d, $J$ = 7.11 Hz, 2H, aromatic). Anal. Calcd for $C_{14}H_{16}F_{12}N_2O_2P_2$: C, 31.47; H, 3.02; N, 5.26. Found: C, 31.43; H, 3.00; N, 5.22.

**10*H*-Phenothiazine-10-propanoic Acid.** This compound was prepared by the procedure of Smith.[8]

**$[Ru(bpy)_2(4,4'\text{-}(CO_2H)_2bpy)](PF_6)_2$.** bpy is 2,2′-bipyridine, and 4,4′-$(CO_2H)_2$bpy is 4,4′-dicarboxy-2,2′-bipyridine. This salt was prepared by the procedure of Wrighton et al.[9]

**$[Ru(bpy)_2(4\text{-}CH_3\text{-}4'\text{-}(CO_2H)bpy)](PF_6)_2$.** 4-$CH_3$-4′-($CO_2H$)bpy is 4-methyl-4′-carboxy-2,2′bpy. This salt was prepared by the procedure of Peek et al.[10]

**$[Ru(bpy)_2(4,4'\text{-}(CO_2^-)_2bpy)]\cdot 2[N(CH_2CH_3)_4][PF_6]$.** This salt was prepared by the literature procedure.[11]

**$[Ru(tpy)(4,4'\text{-}(CO_2H)_2bpy)(H_2O)](ClO_4)_2$.** tpy is 2,2′:6′,2″-terpyridine. This salt was prepared according to the procedure in ref 12 for $[Ru(tpy)(bpy)(H_2O)](ClO_4)_2$. The initial chloro product was converted into the aqua form by heating 0.30 g of the chloro salt and 0.19 g of $AgClO_4$ at reflux for 1 h in 100 mL of 3:1 (v/v) $C_2H_5OH/H_2O$. The solution was filtered, and the volume was decreased to 10 mL and the solution cooled overnight at 5° C. The product was filtered, washed with cold water, and isolated in 97% yield. UV–vis (MeOH): λ(ε) 504 nm ($1.10 \times 10^4$ $M^{-1}$ $cm^{-1}$), 366 nm ($6.79 \times 10^3$ $M^{-1}$ $cm^{-1}$), 310 nm ($3.43 \times 10^4$ $M^{-1}$ $cm^{-1}$). $^1H$ NMR (200 MHz, water-$d_2$): δ 7.28 (m, 3H), 7.52 (d, $J$ = 5.99 Hz, 1H), 7.71 (d, $J$ = 5.48 Hz, 2H), 7.95 (t, $J$ = 7.20 Hz, 2H), 8.23 (t, $J$ = 8.20 Hz, 1H), 8.37 (d, $J$ = 5.80 Hz, 1H), 8.43 (d, $J$ = 8.10 Hz, 2H), 8.58 (d, $J$ = 8.15 Hz, 2H), 8.75 (s, 1H), 9.10 (s, 1H), 9.65 (d, $J$ = 5.61 Hz, 1H). Anal. Calcd for $RuC_{27}H_{23}N_5O_{14}Cl_2$: C, 43.68; H, 3.09; N, 9.43. Found: C, 43.94; H, 3.20; N, 9.37.

**Measurements. Electrochemistry.** Cyclic voltammetric experiments used a PAR 273 potentiostat in conjunction with a PAR 175 universal programmer and a Soltec VP 6414S chart recorder or a PAR 273 with a Hewlett-Packard 7470A plotter. A standard three electrode system was used with either silver/silver nitrate (0.1 M) or SSCE reference electrodes, a platinum-wire counter electrode, and a BAS MF-2013 platinum disk or a derivatized $SnO_2$ or $In_2O_3$ working electrode. Data are reported versus $Ag/AgNO_3$, which was ~350 mV more positive than SSCE. All electrochemical measurements were performed in a nitrogen filled Vacuum/Atmospheres drybox at room temperature unless otherwise noted.

**Electronic Spectroscopy.** Electronic spectra were obtained on a Hewlett-Packard 8451A diode array spectrophotometer in 1-cm cuvettes. Measurements on complexes attached to powdered silica were made through index of refraction matching with cyclohexane or $CH_2Cl_2$. In a typical experiment, silica gel was mixed with the appropriate solvent until a uniform, thick slurry was formed. Several drops of this slurry were transferred to an Aldrich demountable liquid cell and pressed between two quartz windows with a 50-mm teflon spacer. Alternatively, the sample was prepared in an airtight 1-cm glass cuvette.

**Resonance Raman and Infrared Spectroscopy.** Resonance Raman spectra were obtained at the UNC Laser Facility. Laser excitation at 457.9 nm was supplied by a Spectra-Physics 165–05 $Ar^+$ laser and at 406.7 nm by a Coherent INNOVA 90K $Kr^+$ laser. Samples as solids were examined on microscope slides with the laser focused on the sample by using an Olympus microscope equipped with a NEC NC-15 CCD color camera and video display monitor. Scattered radiation was collected by the Raman microprobe system, dispersed by a Jobin Yvon (JY) U1000 (Instruments SA) double monochromator and detected by a thermoelectrically cooled Hamamatsu R943-02 photomultiplier tube. The resulting signal was processed by Instruments SA's Spectra Link photon counting system. Data acquisition was controlled by an IBM PS-2 Model 80 computer with Enhanced Prism Software (Instruments SA).

Solution samples contained in NMR tubes were examined in a spinning arrangement by using two separate experimental setups. One system utilized conventional 90° scattering geometry with the same JY spectrometer and detection system. In the second apparatus Raman scattering was collected in a 135° backscattering geometry into a SPEX 1877 Triplemate equipped with a Princeton Instruments's IRY-700-G optical multichannel analyzer and ST-110 OSMA detector controller. Data acquisition was controlled by an IBM AT computer by utilizing Princeton Instruments software.

Infrared spectra of the Ru salts were recorded as KBr pellets or in acetonitrile solutions between NaCl plates by using a Mattson Galaxy Series FTIR 5000 spectrometer.

**Atomic Force Microscopy.** Several cleaned $SnO_2$:Sb electrodes (from the "old" and "new" batches, see below) were analyzed by using a Nanoscope II atomic force microscope from Digital Instruments, Santa Barbara, CA. The data were resized, filtered, and analyzed by using a Nanoscope III workstation. The root-mean-square (RMS) roughnesses were calculated by software provided by the manufacturer.

**X-ray Photoelectron Spectroscopy.** X-ray photoelectron spectroscopic (XPS) data on several derivatized electrodes were obtained by using a Perkin-Elmer PHI 5400 XPS system equipped with a spherical capacitor energy analyzer. The base operating pressure during analysis ranged from $5 \times 10^{-9}$ to $2 \times 10^{-8}$ Torr. Data for $[Ru(bpy)_2(4,4'\text{-}(CO_2H)_2\text{-}bpy)](PF_6)_2$ attached to ITO electrodes were obtained by using a standard Mg anode as the X-ray source, while an Al source was employed in studies witth PTZ-$CO_2H$ on the electrode surfaces. Binding energies were referenced against the 1s C photoelectron signal set to 285 eV.

**Emission Spectroscopy.** Room temperature, CW emission spectra were recorded on a Spex Fluorolog-F212 emission spectrometer equipped with a 450-W xenon lamp and cooled Hamamatsu GaAs or R928 photomultiplier tubes. Electrodes were placed against the internal front face of a standard cuvette with degassed acetonitrile or dichloromethane


(5) (a) Fujihara, M.; Ohishi, N.; Osa, T. *Nature* **1977**, *268*, 226. (b) Moser, J.; Grätzel, M. *J. Am. Chem. Soc.* **1984**, *106*, 6557.

(6) (a) Fujihara, M.; Kubota, T.; Osa, T. *J. Electroanal. Chem.* **1981**, *81*, 379. (b) Dabestani, R.; Bard, A. J.; Campion, A.; Fox, M. A.; Mallouk, T. E.; Webber, S. E.; White, J. M. *J. Phys. Chem.* **1988**, *92*, 1872. (c) Kalyansundaram, K.; Vlachopoulos, N.; Krishnan, V.; Monnier, A.; Grätzel, M. *J. Phys. Chem.* **1987**, *91*, 2342.

(7) (a) Fox, M. A.; Nobs, F. J.; Voynick, T. A. *J. Am. Chem. Soc.* **1980**, *102*, 4029. (b) Fox, M. A.; Nobs, F. J.; Voynick, T. A. *J. Am. Chem. Soc.* **1980**, *102*, 4036.

(8) Smith, N. L. *J. Org. Chem.* **1950**, *15*, 1125.

(9) Giordano, P. J.; Bock, C. R.; Wrighton, M. S.; Interrante, L. V.; Williams, R. F. X. *J. Am. Chem. Soc.* **1977**, *90*, 3187.

(10) Peek, B. M.; Ross, G. T.; Edwards, S. M.; Meyer, G. J.; Meyer, T. J.; Erickson, B. W. *Int. J. Peptide Protein Res.* **1991**, *38*, 114.

(11) Younathan, J. N.; McClanahan, S. F.; Meyer, T. J. *Macromolecules* **1989**, *22*, 1048.

(12) Takeuchi, K. J.; Thompson, M. S.; Pipes, D. W.; Meyer, T. J. *Inorg. Chem.* **1984**, *23*, 1845.

in the external solution. Emission from solid surfaces was collected in a front face (45°) mode and corrected for the spectral sensitivity of the detector. Control experiments demonstrated that the observed emission originated primarily from the glass backing of the electrodes and was quenched on the electrode surface.

Emission lifetimes were measured following laser flash excitation by using a PRA nitrogen laser Model LN1000 and a PRA dye laser Model LN102. Emission decays were monitored at the emission maximum by using an ISA monochromator Model H-20 and a Hamamatsu R-928 photo tube and recorded on LeCroy 9400 and 7200A digital oscilloscopes interfaced to an IBM-PC. Derivatized ITO samples were mounted with the glass side of the electrode flush against the front face of a standard 1-cm cuvette with DCE in the external solution. Emission decay traces were collected at 45° to the excitation beam. Solution and powdered silica samples were measured 90° to the excitation beam. A solution potassium dichromate filter was employed between sample and monochromator to eliminate scattered light. Traces from 100 laser shots were averaged and collected. Intensity–time decay profiles were fit to either a single exponential decay function[13] or the Williams–Watts (Kolrausch) function in eq 1.[14]

$$I(t) = I_0 \exp\{(-kt)^{\beta}\} \tag{1}$$

The latter function provides a mathematical basis for dealing with a nonsymmetrical distribution of decays and has been successfully employed previously to describe the emission decay of polypyridyl metal complexes immobilized in rigid films and other media.[15] In eq 1, $I_0$ and $I(t)$ are the initial intensity and intensity at time $t$, $k$ is the decay rate constant, and $\beta$ is a constant which reflects the breadth of the nonsymmetrical distribution. If $I(t)$ is interpreted as arising from a distribution of exponential decays, the average lifetime $\langle\tau\rangle$ can be calculated from eq 2, where $\Gamma(n)$ is the $\Gamma$ function.[16]

$$\langle\tau\rangle = \frac{\Gamma(1/\beta)}{k\beta} \tag{2}$$

**Lifetime Quenching.** Lifetime quenching of $[Ru(bpy)_2(4,4'\text{-}(CO_2H)_2\text{-}bpy)](PF_6)_2$ attached to glass was investigated by injecting microliter quantities of a dichloromethane solution 0.1 M in 10-MePTZ (10-MePTZ is 10-methyl-10*H*-phenothiazine) into 5.00 mL of degassed dichloromethane in a sealed cuvette containing the derivatized sample. The results were fit to eq 3a, which was originally derived to explain the solution quenching of protein-bound fluorophors having $n$ different sites.[17] In eq 3a, $I_0$ is the emission intensity in the absence of quencher, $\Delta I$ is the

$$\frac{I_0}{\Delta I} = \left[\sum_{i=1}^{n} \frac{f_i K_{SVi}[Q]}{1 + K_{SVi}[Q]}\right]^{-1} \tag{3a}$$

$$\frac{\langle\tau_0\rangle}{\langle\tau\rangle} = \frac{1}{f_a K_{SV}[Q]} + \frac{1}{f_a} \tag{3b}$$

loss in intensity upon the addition of quencher at concentration [Q], $K_{SVi}$ is the Stern–Volmer constant for emitter $i$, $f_i$ is the fraction of emitters that are $i$, and the summation is over all ($n$) emitters. If it is assumed that there are $m$ accessible emitting sites and $n - m$ inaccessible ones and if lifetime data are used in place of emission intensities, eq 3a simplifies to eq 3b, where $\langle\tau_0\rangle$ and $\langle\tau\rangle$ are the average lifetimes calculated from eq 2 in the absence and presence of quencher, respectively, and $f_a$ ($=\sum f_i$ summed over all $m$) represents the maximum fraction of luminescent sites accessible to quenching.

**Surface Attachment Procedures. Surface Preparation.** For most experiments, the metal oxide electrodes were etched in 10% $HNO_3/H_2O$ (v/v) and rinsed thoroughly in nanopure $H_2O$ before attachment. The $SnO_2$:Sb coatings were etched for 15 min and the $In_2O_3$:Sn coatings for only ~30 s, since they were less stable. Electrodes were brought into a $N_2$-filled glovebox, placed in a standard electrochemical cell, and scanned from 0.0 to +1.7 V in 0.1 M $[N(n\text{-}C_4H_9)_4(PF_6)/CH_2Cl_2$ or $CH_3CN$ to ensure a clean surface.[18]

**Surface Attachment.** In the surface attachment procedure, electrochemically clean electrodes (or glass slides) were soaked in solutions that were $10^{-4}$ M in the carboxylic acid derivative in $CH_3CN$ or $CH_2Cl_2$ with an equal amount of dicyclohexylcarbodiimide (DCC) overnight in a Vacuum Atmosphere drybox. The results of quantitation studies (see below) later showed that surface coverages were complete within 2 h in the absence of DCC, and it was no longer added to the derivatizing solutions. The electrodes were rinsed in neat $CH_3CN$, followed by soaking in 0.1 M $[N(n\text{-}C_4H_9)_4(PF_6)$-$CH_3CN$ for short periods (minutes) to remove any adsorbed salt. These samples were placed in a standard electrochemical cell and examined electrochemically. Derivatized electrodes usually displayed decreased charging currents and new waves for the attached redox couple.

Surface coverages in mol/cm$^2$ of electroactive molecules were quantitated from cyclic voltammograms. After correction for the background charging current for both the positive and negative scans, the areas under voltammetric waves were integrated and divided by the scan rate and electron charge. The moles oxidized and reduced were the same, within the accuracy of the base-line correction, and were independent of scan rate from 10 to 1000 mV/s. Electrode areas were between 0.5 and 3.0 cm$^2$ without correction for surface roughness.

In order to ensure accurate surface area measurements, a series of experiments were conducted involving derivatization of only the center portion of a $SnO_2$:Sb electrode. A glass tube of known diameter containing the derivatizing solution was clamped onto the electrode via a rubber o-ring. The solution was in contact with the electrode for several hours resulting in a circle of electroactive complex at the center of the electrode. The calculated and measured surface coverages were in excellent agreement.

Surfaces which had been derivatized previously could be used again by simply soaking the electrode in an aqueous solution at pH 10 for ~5 min. These electrodes were then rinsed in nanopure water, checked electrochemically for surface contaminants and placed in the derivatizing solution.[19] In general, surface derivatization could be succesfully avoided by coating the electrode (or glass slide) with a thick layer of Type W Apiezon wax prior to exposure to solutions containing the redox or photoactive species.

A sample-dependent complication was observed when $SnO_2$:Sb electrodes were used. With some samples, separate scan-rate independent and dependent Ru(III/II) couples were observed for $[Ru(bpy)_2(4,4'\text{-}(CO_2H)_2bpy)](PF_6)_2$, both with the same half-wave potentials, Figure 1. At fast scan rates, the scan-rate dependent component was resolved from the normal, scan-rate independent surface-attached wave, while at slower scan rates, it fell within the first wave. Initially, this effect was observed rarely and only on samples having large background charging currents. More recently, entire sheets received from the vendor displayed this effect, but only with the Sb-doped material.

In order to investigate this phenomenon further, atomic force microscope (AFM) measurements were conducted on representative examples of the different types of $SnO_2$:Sb samples.[20] Visually, there was an enhanced roughness in the newer samples, Figure 2. The average

(13) Marquardt, D. W. *J. Soc. Ind. Appl. Math.* **1963**, *11*, 431.
(14) Williams, G.; Watts, D. C.; Dev, S. B.; North, A. M. *Trans. Faraday Soc.* **1971**, *67*, 1323.
(15) (a) Jones, W. E., Jr.; Chen, P.; Meyer, T. J. *J. Am. Chem. Soc.* **1992**, *114*, 387. (b) Danielson, E.; Meyer, T. J. Unpublished results.
(16) (a) Lindsey, C. P.; Patterson, G. D. *J. Chem. Phys.* **1980**, *73*, 3348. (b)

$$\Gamma(n) = \int_0^\infty x^{n-1}e^{-x}\,dx = \frac{1}{n}\prod_{m=1}^{\infty}\frac{\left(1+\frac{1}{m}\right)^n}{1+\frac{n}{m}}$$

$n = 1, 2, \ldots$, as defined by: *CRC Handbook of Mathematics*; CRC Press: Boca Raton, FL.
(17) Lehrer, S. S. *Biochemistry* **1971**, *10*, 3254.

(18) Electrodes cleaned in this manner displayed only charging currents and the onset of solvent oxidation at >1.7 V. For a 1 cm$^2$ electrode, charging currents were typically 20 μA for $SnO_2$:Sb and ~10 μA for $In_2O_3$:Sn at a scan rate of 200 mV/s. The charging currents increased directly with increasing scan rate. If an electrode displayed any waves due to impurities it was soaked in aqueous 10% KOH solution for 5 min, rinsed in nanopure $H_2O$, etched in 10% $HNO_3/H_2O$ (v/v), and rinsed again thoroughly in nanopure $H_2O$.
(19) Samples which had been etched several times began to display increased charging currents and a larger variability in final surface coverage. The $SnO_2$:Sb surfaces proved to be extremely resilient to continued etching and multiple surface attachment cycles. These electrodes were used routinely in 10–20 surface attachment cycles. The tin-doped indium oxide was less resistant and could only be used for two or three cycles. The surface stability in a $N_2$ filled drybox was noticeably improved compared to surfaces derivatized in the ambient atmosphere of the laboratory.
(20) Binnig, G.; Quate, C. F.; Gerber, C. *Phys. Rev. Lett.* **1986**, *56*, 930.

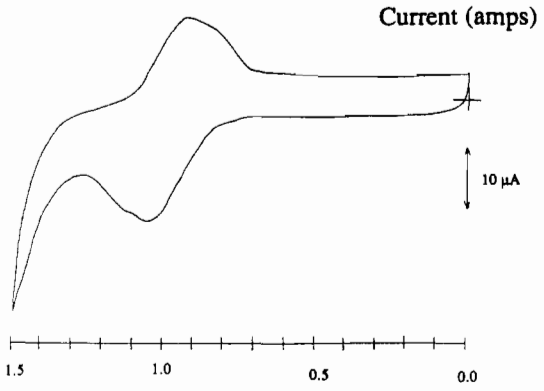


**Figure 1.** Cyclic voltammogram at a scan rate of 100 mV/s for [Ru(bpy)$_2$(4,4′-(CO$_2$H)$_2$bpy)](PF$_6$)$_2$ attached to a "new" SnO$_2$:Sb electrode in 0.1 M [N(*n*-C$_4$H$_9$)$_4$(PF$_6$) in dichloromethane.

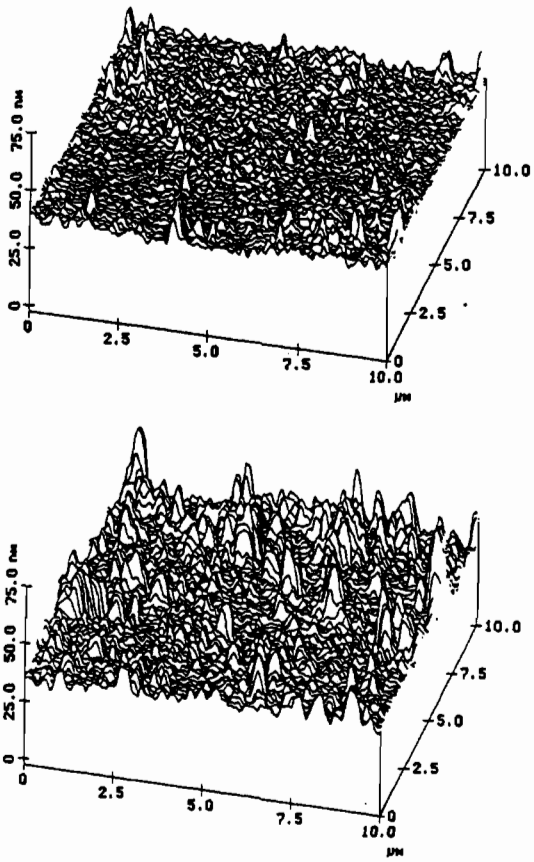


**Figure 2.** Atomic force microscopy photographs of "old" (top) and "new" (bottom) SnO$_2$:Sb electrodes, as received from the vendor.

root-mean-square (rms) roughness of the older batch of electrodes was 4.2 nm. The newer electrodes have more frequent and larger features, as indicated by a higher rms roughness of 6.5 nm. Line plots for the two samples are shown in Figure 2. On the rougher samples there may be a second type of binding site which displays considerably slower electron transfer kinetics.

**Mixed Surfaces.** Mixed surfaces were prepared by either sequential or competitive binding. In the sequential procedure, the substrate was soaked in a solution containing the first carboxylic acid-containing molecule, removed before coverage was complete, and soaked in a solution containing the second molecule until surface coverage was complete. In the competitive procedure, both carboxylic acid-containing molecules were present in the derivatizing solution and competitive surface binding proceeded until complete coverage was reached. The relative surface coverages of the attached groups were established by cyclic voltammetry. Surfaces with varying ratios of bound molecules were fabricated by varying the soaking time in the initial solution for the sequential procedure or the relative solution concentrations in the second procedure.

**Quantitation of Surface Binding.** Electrodes used for the quantitation of surface binding were first etched in concentrated sulfuric acid for 1 h, rinsed in nanopure water, soaked in 50% NaOH for 1 h, and rinsed in nanopure water, followed by methanol and finally acetone. Solutions $10^{-4}$–$10^{-10}$ M in [Ru(bpy)$_2$(4,4′-(CO$_2$H)$_2$bpy)](PF$_6$)$_2$ in CH$_2$Cl$_2$ were prepared by dilutions of stock solutions. Concentrations were verified spectrophotometrically. Standardized solutions were placed in vials and a 1 cm$^2$ surface area of the electrodes was exposed. The surface reaction was allowed to proceed for at least 2 h. The electrodes were rinsed and examined by electrochemical measurements.

**SiO$_2$ Powders.** Colloidal silica (Cabosil) and silica catalyst support (Aldrich; grade 951) were used as received or initially dried under vacuum at 100 °C for 24 h. These supports were coated by creating a slurry with $10^{-3}$ M [Ru(bpy)$_2$(4,4′-(CO$_2$H)$_2$bpy)](PF$_6$)$_2$ and DCC in CH$_3$CN and stirring overnight. The modified supports were repeatedly rinsed in 0.1 M [N(*n*-C$_4$H$_9$)$_4$(PF$_6$)-CH$_3$CN and centrifuged, and the supernatant was checked for free complex. Once the supernatant displayed no free complex, the solid was dried in air or with gentle heating.

**SnO$_2$ and TiO$_2$ Powders.** Powdered SnO$_2$ (Aldrich; 99.99%) and TiO$_2$ (Aldrich; 99.9%) were used as received. These supports were derivatized by creating a slurry with ~$10^{-4}$ M [Ru(bpy)$_2$(4,4′-(CO$_2$H)$_2$bpy)](PF$_6$)$_2$ and DCC in CH$_3$CN with stirring overnight. The modified supports were centrifuged and repeatedly rinsed with neat CH$_3$CN. The solids were dried in air or with gentle heating.

## Results

The structures and abbreviations of the ligands and of the phenothiazine and bipyridine carboxylic acid derivatives are illustrated as follows:

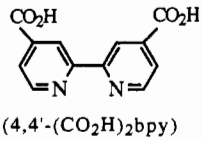


(4,4′-(CO$_2$H)$_2$bpy)

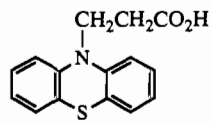


(PTZ-CO$_2$H)

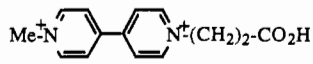


(MV$^{2+}$-CO$_2$H)

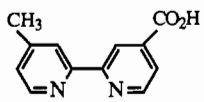


(4-CH$_3$-4′-(CO$_2$H)bpy)

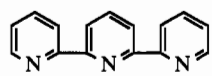


(tpy)

**Binding to SnO$_2$, In$_2$O$_3$, and SiO$_2$.** Typical cyclic voltammograms of 10*H*-phenothiazine-10-propanoic acid, 3-(1′-methyl-4,4′-bipyridinium-1-yl)propanoic acid, [Ru(bpy)$_2$(4,4′-(CO$_2$H)$_2$-bpy)](PF$_6$)$_2$, and [Ru(tpy)(4,4′-(CO$_2$H)$_2$bpy)(H$_2$O)](PF$_6$)$_2$ attached to SnO$_2$:Sb as a function of scan rate are shown in Figure 3. Data for complexes attached to In$_2$O$_3$:Sn gave similar $E_{1/2}$ values, but the wave forms were slightly sharper. Reproducible cyclic voltammograms were obtained for the attached couples, and their $E_{1/2}$ values were nearly the same as for the couples in solution at a Pt electrode (Table 1). The peak currents for these waves varied directly with scan rate in all cases, as expected for a surface confined complex in the absence of diffusion.[21]

A limiting surface coverage of ~1.1 × $10^{-10}$ mol/cm$^2$ for [Ru(bpy)$_2$(4,4′-(CO$_2$H)$_2$bpy)]$^{2+}$ can be calculated if spheres of

(21) Bard, A. J.; Faukner, L. R. *Electrochemical Methods*; John Wiley & Sons, Inc.: New York, 1980.

**Table 1.** Absorption, Emission, and Electrochemical Properties in $CH_3CN$ at 298 K

| compound or salt | redox couple | $\lambda_{abs}$,[a] nm | $\lambda_{em}$,[b] nm | $E_{1/2}$, V solution[c] | $E_{1/2}$, V $SnO_2$:Sb[d] | $E_{1/2}$, V $In_2O_3$:Sn[d] |
|---|---|---|---|---|---|---|
| $[Ru(bpy)_2(4,4'\text{-}(CO_2H)_2bpy)](PF_6)_2$ | Ru(III/II) | 474 | 680 | 1.03 | 1.03 | 0.99 |
| $[Ru(bpy)_2(4,4'\text{-}(CO_2^-)_2bpy)]\cdot 2[N(C_2H_5)_4](PF_6)$ | Ru(III/II) | 454 | 639 | 0.83[e] | | |
| $[Ru(bpy)_2(4,4'\text{-}(CO_2CH_2CH_3)_2bpy)](PF_6)_2$ | Ru(III/II) | 478 | 687 | 1.05 | | |
| $[Ru(bpy)_2(4\text{-}(CH_3),4'\text{-}(CO_2H)bpy)](PF_6)_2$ | Ru(III/II) | 462 | 673 | 1.00 | 1.02 | 0.97 |
| $[Ru(tpy)(4,4'\text{-}(CO_2H)_2bpy)(H_2O)](PF_6)_2$ | Ru(III/II) | 534 | | 0.56 | 0.64 | 0.62 |
| 3-(10H-phenanthiazine-9)propanoic acid | $-PTZ^{+/0}$ | | | 0.41 | 0.42 | |
| 3-(1′-methyl-4,4′-bipyridinium-1)propanoic acid | $-MV^{2+/+}$ | | | −0.71 | −0.88 | |
| $[Os(bpy)_2(4,4'\text{-}(CO_2H)_2bpy)](PF_6)_2$ | Os(III/II) | 498 | 832 | 0.63 | | 0.55 |
| $[Ru(bpy)_2(4,4'\text{-}(CO_2H)_2bpy)](PF_6)_2/SiO_2$[f] | | 464 | 658 | | | |

[a] $\lambda_{max}$ for the lowest intense MLCT feature. [b] Emission maximum with excitation at 460 nm. [c] Half-wave potentials were obtained by cyclic voltammetry and are reported as V vs Ag/$AgNO_3$ (0.1 M), which was ~350 mV vs SSCE in acetonitrile 0.1 M in $[N(n\text{-}C_4H_9)_4](PF_6)$ by using ferrocene as an internal standard. The solution values were measured at a Pt working electrode. [d] For the couple attached to the indicated electrode. [e] For $[Ru(bpy)_2(4,4'\text{-}(CO_2H)_2bpy)](PF_6)_2$ in acetonitrile, deprotonated by the addition of triethylamine, an irreversible oxidation wave appears at $E_p \sim 0.80$ V. [f] For $[Ru(bpy)_2(4,4'\text{-}(CO_2H)_2bpy)](PF_6)_2$ on powdered $SiO_2$, with 1,2-dichloroethane as the external solvent for index of refraction matching.

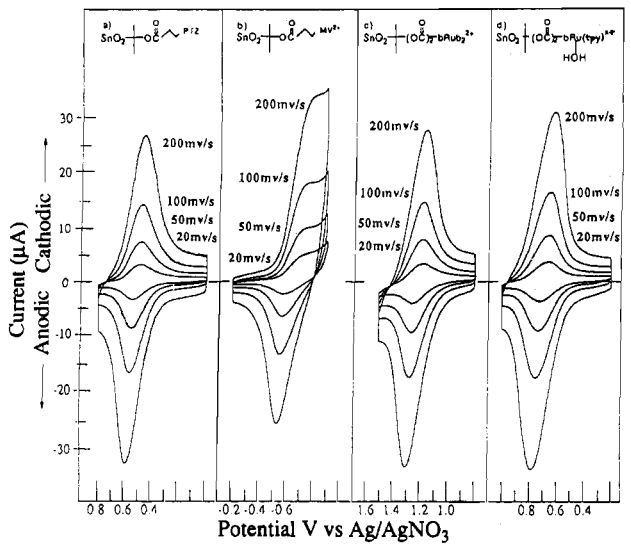


**Figure 3.** Cyclic voltammograms at the indicated scan rates for molecular assemblies of four different redox acids attached to 1.5 $cm^2$ $SnO_2$:Sb electrodes. Cyclic voltammograms were obtained in 0.1 M $[N(n\text{-}C_4H_9)_4](PF_6)$ in dichloromethane for (*a*) 10*H*-phenothiazine-10-propanoic acid; (b) 3-(1′-methyl-4,4′-bipyridinium-1-yl)propanoic acid, (c) $[Ru(bpy)_2(4,4'\text{-}(CO_2H)_2bpy)](PF_6)_2$, and (d) $[Ru(tpy)(4,4'\text{-}(CO_2H)_2bpy)(H_2O)](PF_6)_2$.

7 Å radii (estimated by using van der Waals radii) are closely packed on a flat surface, neglecting the $PF_6^-$ counterions. Limiting surface coverages in the range $(0.5\text{–}1.0) \times 10^{-10}$ mol/$cm^2$ were measured for a large number (>100) of electrodes derivatized by attachment of $[Ru(bpy)_2(4,4'\text{-}(CO_2H)_2bpy)](PF_6)_2$. The limiting surface coverages for other redox couples were generally within the same range. The exception was $[Ru(tpy)(4,4'(CO_2H)_2bpy)(H_2O)](PF_6)_2$, for which surface coverages as high as $1 \times 10^{-9}$ mol/$cm^2$ were reproducibly obtained when high concentrations ($>10^{-4}$ M) of the salt in methanol were exposed to the surface. Prolonged soaking of these derivatized surfaces in concentrated salt solutions did not result in a rapid decrease in surface coverage as was the case for molecules present by physical adsorption.

Attempts were made to follow the kinetics of surface binding on $SnO_2$:Sb electrodes in acetonitrile solutions $2 \times 10^{-5}$ M in $[Ru(bpy)_2(4,4'\text{-}(CO_2H)_2bpy)](PF_6)_2$ in $CH_3CN$ with and without DCC. The results of these studies were highly inconsistent. Side-by-side experiments performed under identical conditions displayed dramatic variations in the amount of time necessary to achieve full surface coverage. In the extremes, complete surface coverages were attained in times as short as 30 s and as long as 1 h in the presence or absence of DCC. Generally, limiting surface coverages were attained within 15 min. More consistent results were obtained with $CH_2Cl_2$ as the solvent in the absence of DCC.

Nonzero peak to peak splittings were routinely observed for the surface-attached couples. The origin of the effect appears not to be in uncompensated solution resistance. Increasing the electrolyte concentration to saturation, increasing the counter electrode surface area, stirring the electrolyte, or altering the electrode geometry had no effect on the magnitude of the peak-to-peak splitting. By inference, the effect arises from slow electron transfer kinetics across the semiconducting oxide interface.

**Surface Attachment and Stability.** The stability of the surface-attached couples, as judged by loss of the surface electrochemical waves, is dependent on the couple, the electrode, and the conditions under which the electrochemistry is performed. When a freshly prepared, derivatized electrode was placed in an electrolytic solution and examined electrochemically, peak currents decreased on scanning—more notably on the first 1–5 scans than the subsequent 30 scans. Quantitative measurements were made after the initial scans when the voltammograms were essentially reproducible on consecutive scans.

Surface stabilities were greater for attachment reactions which proceeded for >24 h compared to those which proceeded less than 2 h. Although surface binding may initially be rapid, a slower surface rearrangement may take place on the time scale of hours, which results in a more stable surface structure. Evidence for this type of surface behavior has recently been demonstrated for sodium laurate binding to $Al_2O_3$.[22] Instability on the surface is induced, at least in part, by redox cycling through the higher oxidation state. For example, for $[Ru(bpy)_2(4,4'\text{-}(CO_2H)_2bpy)](PF_6)_2$ attached to a $SnO_2$:Sb electrode, biasing the electrode at +0.3 V in $[N(n\text{-}C_4H_9)_4(PF_6)/CH_2Cl_2$, where the complex is Ru(II), resulted in < 2% loss in peak current after 1 h. After holding the potential at +1.1 V, where the complex is Ru(III), an ~80% loss was observed after 1 h. Potential hold experiments with other surface-attached couples displayed related phenomena. Thus, measurement of surface coverages by cyclic voltammetry is dependent on the potential limits and the time spent in an oxidized or reduced state and the measurement itself contributes to the irreproducibility.

Under ideal conditions in dry organic solvents the loss of peak current for the Ru(III/II) wave of $[Ru(bpy)_2(4,4'\text{-}(CO_2H)_2bpy)](PF_6)_2$ was less than 10% after 1 h of cycling over the potential range 0.0–1.4 V at 200 mV/s. More typically, the loss of surface-attached complex was 30–40%. A single reductive scan into the first bpy-based reduction wave at −1.6 V resulted in complete loss of the surface Ru(III/II) wave on a following scan. The surface-attached groups were rapidly removed by aqueous base (pH = 10). Only $[Ru(tpy)(4,4'\text{-}(CO_2H)_2bpy)(H_2O)](ClO_4)_2$ exhibited some resistance to stripping with added base.

Addition of water to acetonitrile or dichloromethane solutions increased the rate of surface loss on oxidative scanning and moisture in the air may be the origin of the decreased stability

(22) Couzis, A.; Gulari, E. *Langmuir* **1993**, *9*, 3414.
(23) Langmuir, I. *J. Amer. Chem. Soc.* **1918**, *40*, 1361.

of electrodes derivatized in the atmosphere compared to the drybox. The mono(carboxylic acid) salt $[Ru(bpy)_2(4\text{-}CH_3\text{-}4'\text{-}(CO_2H)bpy)](PF_6)_2$ also attaches to $SnO_2$ with a maximum surface coverage of $\sim 1 \times 10^{-10}$ mol/cm$^2$. Electrochemical measurements demonstrate that the resulting assembly is comparable in stablity toward oxidative cycling as assemblies of the corresponding diacid complex. Surface-bound $[Ru(tpy)(4,4'\text{-}(CO_2H)_2bpy)(H_2O)]^{2+}$ displays a surface stability toward redox cycling through the Ru(III/II) couple which is comparable to the diacid complex.

The $MV^{2+/+}$–$CO_2H$ couple displayed the worst surface stability. In the best cases, the loss of peak current was ~3 % per cycle from 0.0 to −1.1 to 0.0 V. These assemblies were highly water sensitive and electrochemical measurements were performed in the drybox. Scans through the second $MV^{2+}$–$CO_2H$ wave at −1.1 V resulted in even more rapid loss of the couple from the surface. The PTZ-$CO_2H$ derivative also forms assemblies on $SnO_2$:Sb, with XPS peaks at ~400.1 and 163.8 eV, respectively, for the 1s (N) and 2p (S) binding energies. Upon scanning between −0.3 and +0.5 V, the surface stability of the couple was comparable, but slightly worse than for $[Ru(bpy)_2(4,4'\text{-}(CO_2H)_2\text{-}bpy)](PF_6)_2$. When the scans were extended into the second PTZ oxidation wave at $E_{p,a} \sim 0.8$ V, complete loss of the surface couples occurred. Additionally, a second XPS sulfur peak with a binding energy of 168.9 eV was observed which qualitatively increased as a function of redox cycling time, consistent with the formation of the sulfoxide on the electrode surface. The origin of the O-atom in the sulfoxide is presumably due to trace $H_2O$ in the solvent, eq 4.

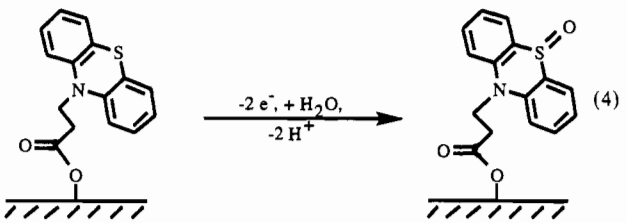


(4)

Exposure of $SnO_2$:Sb or $In_2O_3$:Sn electrodes to a solution $10^{-4}$ M in $[Ru(bpy)_3](PF_6)_2$ in acetonitrile gave no evidence for surface attachment. Addition of DCC or electrolyte to the solution did not alter the observation. For $[Ru(tpy)(4,4'\text{-}(CO_2H)_2bpy)(H_2O)]^{2+}$ bound to $SnO_2$:Sb, the Ru(III/II) wave displayed a pH dependence comparable to that for the $[Ru^{III}(tpy)(bpy)(OH)]^{2+}/[Ru^{II}(tpy)(bpy)(H_2O)]^{2+}$ couple below pH 4.[12] This couple is independent of pH below pH ~ 3.0 with $E_{1/2} = 0.84$ V. Above this pH, the Ru(III/II) wave decreases ~59 mV/pH unit as expected, but is slowly removed from the surface. The lack of surface stability as the pH was raised made quantitative measurements difficult. No evidence for a wave arising from the surface-bound analog of the $[Ru^{IV}(tpy)(bpy)(O)]^{2+}/[Ru^{III}(tpy)(bpy)(OH)]^{2+}$ couple was found. A special feature of the surface-bound complex was slow substitution of water by acetonitrile. After 10 days of soaking in $CH_3CN$, only 5% of the attached aqua complex had undergone solvolysis as demonstrated by the appearance of a wave for the $[Ru(tpy)(4,4'(CO_2H)_2bpy)(CH_3CN)]^{3+/2+}$ couple at 1.2 V. The rate constant for solvolysis of $[Ru(tpy)(4,4'\text{-}(CO_2H)_2bpy)(H_2O)]^{2+}$ in $CH_3CN$ at 25 °C is $k = 1.9 \times 10^{-4}$ s$^{-1}$ ($t_{1/2} \sim 1$ h) by spectrophotometric measurements.

**Raman Spectroscopy.** Resonance Raman spectra (1000–1750 cm$^{-1}$) for $[Ru(bpy)_2(4,4'\text{-}(CO_2H)_2bpy)](PF_6)_2$ in $H_2O$ at pH 1.8 and pH 6.0 and of $[Ru(bpy)_2(4,4'\text{-}(CO_2Et)_2bpy)](PF_6)_2$ in $CH_2Cl_2$ are shown in Figure 4. At pH 6, the dominant form of the complex is $[Ru(bpy)_2(4,4'\text{-}(CO_2^-)_2bpy)]$. Spectra of $[Ru(bpy)_2(4,4'\text{-}(CO_2H)_2bpy)](PF_6)_2$ attached to $SiO_2$ and $SnO_2$ powders are shown in Figure 5. The Raman spectrum on $TiO_2$ is nearly identical to the spectrum on $SnO_2$. For the measurements on

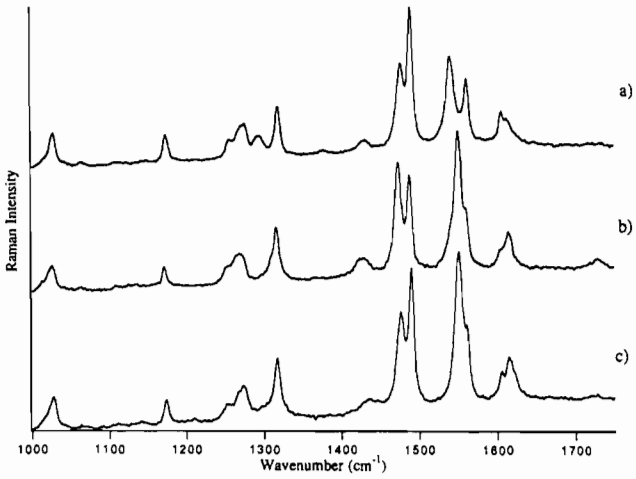


**Figure 4.** Resonance Raman spectra between 1000 and 1750 cm$^{-1}$ for (a) $[Ru(bpy)_2(4,4'\text{-}(CO_2H)_2bpy)](PF_6)_2$ at pH = 6, (b) $[Ru(bpy)_2(4,4'\text{-}(CO_2Et)_2bpy)](PF_6)_2$ in dichloromethane, and (c) $[Ru(bpy)_2(4,4'\text{-}(CO_2H)_2bpy)](PF_6)_2$ at pH = 1.8. The excitation wavelength was 457.9 nm with ~30 mW at the sample and a spectral resolution of 4 cm$^{-1}$.

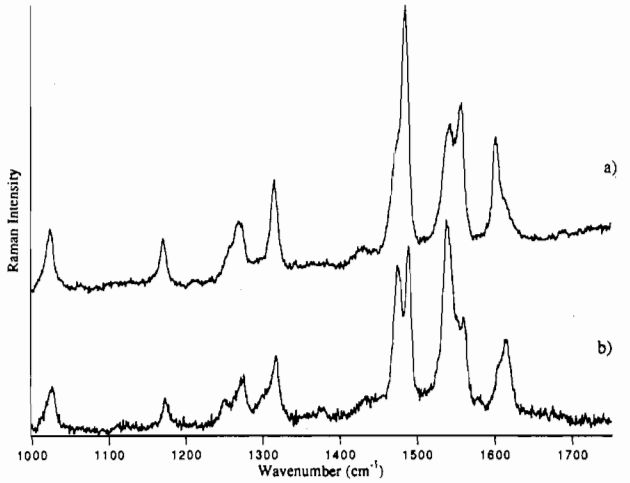


**Figure 5.** (a) Resonance Raman spectrum of $[Ru(bpy)_2(4,4'\text{-}(CO_2H)_2\text{-}bpy)](PF_6)_2$ attached to powdered $SnO_2$. The excitation wavelength was 457.9 nm with ~5 mW of laser power by utilizing a Raman microprobe apparatus. (b) Spectrum of $[Ru(bpy)_2(4,4'\text{-}(CO_2H)_2bpy)](PF_6)_2$ attached to $SiO_2$ dispersed in $CCl_4$ obtained in a NMR tube, with 90° sampling geometry and ~20 mW laser power at the sample. This spectrum was corrected for background emission.

$SiO_2$ the sample was dispersed in carbon tetrachloride (for refractive index matching) which gave transparent orange solutions. Identical spectra were obtained for this sample as a solid, dispersed in aqueous solution at pH 1.4, or dispersed in $CCl_4$. The baseline was corrected for the strongly emissive background from samples on $SiO_2$. The energies of relevant Raman bands between 1000 and 1750 cm$^{-1}$ are presented in Table 2. In general, all Raman measurements were conducted on samples that were soaked in the derivatization solutions for extended periods and were assumed to be thermally and kinetically equilibrated.

**Surface Binding and Exchange.** The thermodynamics of surface binding were investigated by electrochemical measurements on electrodes that had reached equilibrium with external solutions containing varying concentrations of $[Ru(bpy)_2(4,4'\text{-}(CO_2H)_2\text{-}bpy)](PF_6)_2$. The results of a representative study are shown in Figure 6 as a plot of the fractional surface coverage, $\theta$ ($=\Gamma/\Gamma_0$ where $\Gamma_0$ is the maximum coverage, $1 \times 10^{10}$ mol/cm$^2$) vs the concentration of Ru(II) in the external dichloromethane solution. A plot of $\theta^{-1}$ vs $[Ru(II)]^{-1}$ is shown in the inset in Figure 6.

From the Langmuir model for surface adsorption,[23] $\theta$ is predicted to vary with [Ru(II)] as shown in eq 5, where $K$ is the

**Table 2.** Raman Bands ($cm^{-1}$) with 457.9- or 454.5-nm Excitation

| $[Ru(bpy)_3]^{2+}$ ($H_2O$, pH = 7) | $[Ru(bpy)_2(4,4'(CO_2Et)_2bpy)]^{2+}$ ($CH_2Cl_2$) | $[Ru(bpy)_2(4,4'-(CO_2H)_2bpy)]^{2+}$ pH = 1.8 | pH = 6.0 | on $SiO_2$[b] | on $SnO_2$ or $TiO_2$[c] | assignt[a] |
|---|---|---|---|---|---|---|
| 1025 | 1025 | 1026 | 1026 | 1025 | 1025 | $\nu_{15}$, $\nu_{15}'$ |
| 1062 | 1061 | 1063 | 1063 | | | $\nu_{14}$ |
| 1104 | 1106 | 1107 | 1108 | | | $\nu_{13}$ |
| 1171 | 1171 | 1172 | 1171 | 1172 | 1172 | $\nu_{12}$, $\nu_{12}'$ |
| 1264[d] | 1254 | 1253 | 1254 | 1249 | 1256 | $\nu_{11}$, $\nu_{11}'$ |
| 1272 | 1270 | 1273 | 1272 | 1273 | 1270 | $\nu_{10}$, $\nu_{10}'$ |
| | | | 1292 | 1305 | | $\nu_{sym}$ (COO) |
| 1316 | 1315 | 1317 | 1316 | 1316 | 1315 | $\nu_9$, $\nu_9'$ |
| | | | 1374 | 1377 | | |
| 1428 | 1428 | 1433 | 1429 | 1433 | 1431 | $\nu_8$, $\nu_8'$ |
| | 1472 | 1475 | 1475 | 1474 | 1473 | $\nu_7'$ |
| 1488 | 1487 | 1489 | 1489 | 1489 | 1486 | $\nu_7$ |
| | 1549 | 1550 | 1540 | 1538 | 1544 | $\nu_6'$ |
| 1559 | 1559 | 1558 | 1560 | 1560 | 1556 | $\nu_6$ |
| 1605 | 1604 | 1605 | 1606 | 1604 | 1604 | $\nu_5$ |
| | 1614 | 1615 | 1615 | 1615 | 1613 | $\nu_5'$ |
| | 1730 | 1725 | | | 1691 | $\nu$(C=O) |

[a] Assignments from refs 28 and 29b (see text). The primes denote bands for the non-bpy ligand. [b] Spectrum on powdered silica suspended in $CCl_4$ for index of refraction matching. [c] Spectra on powdered samples. [d] Shoulder.

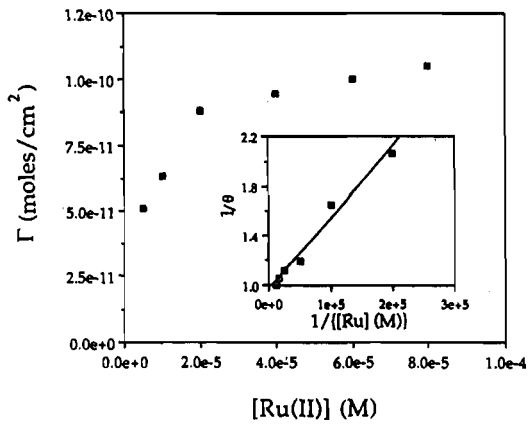


**Figure 6.** Surface coverage versus solution concentration for $[Ru(bpy)_2(4,4'-(CO_2H)_2bpy)](PF_6)_2$ attached to $In_2O_3$:Sn. The points represent surface coverages determined electrochemically. A double reciprocal plot of the data expressed as fractional surface coverage ($\theta$, see text) is shown in the inset.

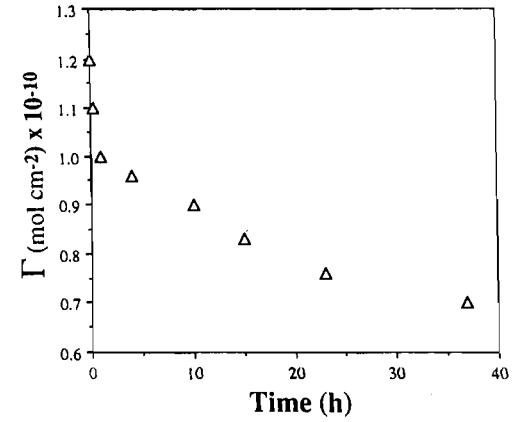


**Figure 7.** Results of a surface exchange experiment showing loss of $[Ru(bpy)_2(4,4'-(CO_2H)_2bpy)](PF_6)_2$ (initially $1.1 \times 10^{-10}$ mol/cm²) with $10^{-5}$ M $[Ru(tpy)(4,4'-(CO_2H)_2bpy)(H_2O)](PF_6)_2$ in the external solution. The growth in the Ru(III/II) wave for the aqua couple was concomitant.

equilibrium constant for binding to the surface. From the inverse-inverse plot in the inset in Figure 6, and eq 6, $K = (8 \pm 6) \times 10^4$ $M^{-1}$ on $In_2O_3$:Sn and $SnO_2$:Sb for $[Ru(bpy)_2(4,4'-(CO_2H)_2bpy)](PF_6)_2$ in dichloromethane at 293 K. The magnitude of $K$ was not influenced by the presence of 0.1 M $[N(n\text{-}C_4H_9)_4](PF_6)$ or equimolar quantities of DCC in the derivatizing solution.

$$\theta = \frac{K[Ru^{II}]}{1 + K[Ru^{II}]} \quad (5)$$

$$\frac{1}{\theta} = 1 + \frac{1}{K[Ru^{II}]} \quad (6)$$

A series of experiments were conducted in order to explore the question of exchange of one redox active group by another. In Figure 7 are shown the results of a typical surface exchange experiment. In this experiment, a $SnO_2$:Sb electrode derivatized with $1.1 \times 10^{-10}$ mol/cm² of $[Ru(bpy)_2(4,4'-(CO_2H)_2bpy)](PF_6)_2$ was placed in a methanol solution $10^{-5}$ M in $[Ru(tpy)(4,4'-(CO_2H)_2bpy)(H_2O)](PF_6)_2$. The sample was periodically removed and relative surface coverages measured by the electrochemical method in dichloromethane 0.1 M in $[N(n\text{-}C_4H_9)]_4(PF_6)$. The loss of $[Ru(bpy)_2(4,4'-(CO_2H)_2bpy)](PF_6)_2$ and the growth of $[Ru(tpy)(4,4'-(CO_2H)_2bpy)(H_2O)](PF_6)_2$ were concomitant; the sum of the surface coverages was equal to the total initial surface coverage, within experimental error.

The results of the exchange reactions can be summarized as follows. For electrodes that were derivatized for extended periods (hours), an initial rapid, <1 h, exchange takes place, followed by a slower exchange which continues for weeks. For the data shown in Figure 7, ~20 % exchange occurred in the first hour and 30% over the next 35 h. Qualitatively, the exchange of $[Ru(tpy)(4,4'-(CO_2H)_2bpy)(H_2O)]^{2+}$ for $[Ru(bpy)_2(4,4'-(CO_2H)_2bpy)]^{2+}$ and the reverse exchange were reproducible, but the rate and percentage of initial exchange were highly sample dependent. Exchange on surfaces that had been derivatized for short periods (seconds) underwent exchange rapidly in $CH_3OH$ and more slowly in dry $CH_2Cl_2$. Surface exchange reactions between PTZ-$CO_2H$ and MV-$CO_2H^{2+}$ were studied less extensively, but had the same qualitative features.

**Mixed Surfaces.** A series of experiments were conducted in order to establish the potential of the oxide linkage chemistry for preparing complex surface assemblies in which more than one redox couple was bound. In Figure 8 are illustrated cyclic voltammograms of bicomponent assemblies prepared by either the competitive or sequential binding techniques (Experimental Section). The assembly in panel a was prepared by first exposing the electrode to a solution $2 \times 10^{-4}$ M in $[Ru(bpy)_2(4,4'-(CO_2H)_2bpy)](PF_6)_2$ and $10^{-4}$ M in DCC in $CH_3CN$ for 1 min and then transferring it to a solution that was $10^{-5}$ M in $[Ru(tpy)(4,4'-(CO_2H)_2bpy)(H_2O)](PF_6)_2$ in MeOH overnight. The voltammogram in panel b was obtained for an electrode that was exposed to a solution ~$10^{-4}$ M each in 10*H*-phenothiazine-10-propanoic

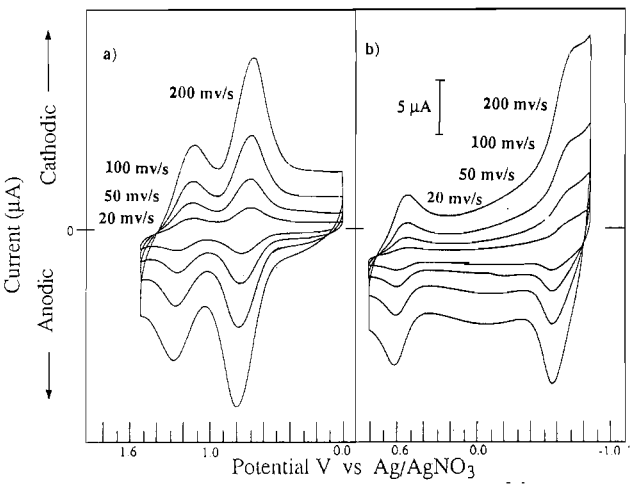


**Figure 8.** Cyclic voltammograms with conditions as in Figure 3 for electrodes with (a) bound $[Ru(bpy)_2(4,4'\text{-}(CO_2H)_2bpy)](PF_6)_2$ ($3.7 \times 10^{-11}$ mol/cm$^2$) and $[Ru(tpy)(4,4'\text{-}(CO_2H)_2bpy)(H_2O)](PF_6)_2$ ($8.3 \times 10^{-11}$ mol/cm$^2$) and (b) 10*H*-phenothiazine-10-propanoic acid ($2.8 \times 10^{-11}$ mol/cm$^2$ and 3-(1′-methyl-4,4′-bipyridinium-1-yl)propanoic acid ($7.3 \times 10^{-11}$ mol/cm$^2$).

acid, 3-(1′-methyl-4,4′-bipyridinium-1-yl)propanoic acid, and DCC in $CH_3CN$ overnight.

In general, the competitive procedure proved to be the preferred method. The sequential procedure always resulted in a degree of surface exchange which has highly sample dependent, and it was difficult to prepare samples with the same relative final surface coverages reproducibly. The sequential procedure could be utilized repetitively to control relative surface coverage. For example, surface-attached $[Ru(bpy)_2(4,4'\text{-}(CO_2H)_2bpy)](PF_6)_2$ in Figure 8a could be increased relative to $[Ru(tpy)(4,4'\text{-}(CO_2H)_2bpy)(H_2O)](PF_6)_2$ by placing the electrode back in the original $[Ru(bpy)_2(4,4'\text{-}(CO_2H)_2bpy)](PF_6)_2$ solution. The competitive procedure reproducibly gave the same relative surface coverages for two electrodes placed in the same solution within experimental error, with or without added 0.1 M $[N(n\text{-}C_4H_9]_4(PF_6)$. In general, solution and surface compositions were not the same when there were structural differences between the competitors. An example of this is shown in Figure 8b where equimolar solution concentrations led to a surface ratio of ~2.6:1.

Analysis of the mixed PTZ–Ru(II) surfaces by cyclic voltammetry was complicated by the fact that an oxidative scan to the Ru(III/II) wave resulted in the loss of the $-PTZ^{+/0}$ wave because, as noted above, at this potential –PTZ undergoes a second oxidation to give the sulfoxide. In the electrochemical experiments, the amount of –PTZ attached was first measured and, subsequently, the amount of Ru. In cases where photophysical experiments were conducted on the glass backing of the electrodes, electrochemical measurements on the metal oxide side were conducted after the photophysical measurements were completed.

**Photophysical and Photochemical Properties.** In Figure 9 are shown UV–vis spectra of the protonated and deprotonated forms of $[Ru(bpy)_2(4,4'\text{-}(CO_2H)_2bpy)](PF_6)_2$ in acetonitrile solution and the same salt attached to silica gel acquired with $CH_2Cl_2$ or 1,2-dichloroethane in the external solution for index of refraction matching. The lowest metal-to-ligand charge transfer (MLCT) absorptions for these complexes are at $\lambda_{max}$ = 474, 454, and 462 nm, respectively. A characteristic feature of polypyridyl complexes of Ru(II) is the appearance of emission from low-lying Ru(II) → bpy MLCT excited states.[24] Table 1 lists emission maxima (460-nm excitation) for $[Ru(bpy)_2(4,4'\text{-}(CO_2H)_2bpy)](PF_6)_2$, $[Ru(bpy)_2(4,4'\text{-}(CO_2\text{-})_2bpy)]\cdot 2[N(CH_2CH_3)_4][PF_6]$, and $[Ru(bpy)_2(4,4'\text{-}(CO_2)_2bpy)](PF_6)_2$ in acetonitrile solution. These

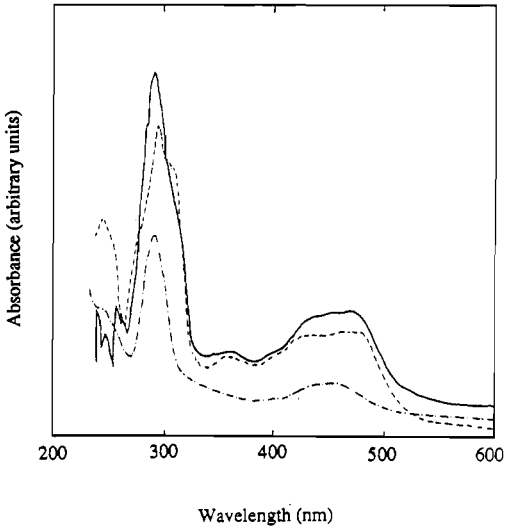


**Figure 9.** Absorption spectra of the protonated (- - -) and deprotonated (– • –) forms of $[Ru(bpy)_2(4,4'\text{-}(CO_2H)_2bpy)](PF_6)_2$ in $CH_3CN$ and of the complex attached to powdered silica (—) with external 1,2-dichloroethane for index of refraction matching.

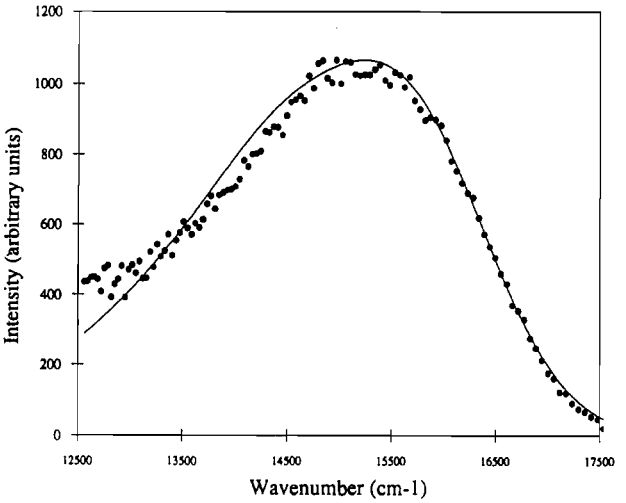


**Figure 10.** Corrected emission spectrum (460 nm excitation wavelength, 45° front face geometry, solid circles) and fitted spectrum[36] (solid line) of the glass side of an $In_2O_3$:Sn electrode derivatized with $[Ru(bpy)_2(4,4'\text{-}(CO_2H)_2bpy)](PF_6)_2$ with acetonitrile as the external solvent.

results parallel previous studies in water where the maximum shifts to higher energy upon deprotonation of the $bpy(CO_2H)_2$ ligand.[25]

Figure 10 shows a typical emission spectrum (460-nm excitation) of $[Ru(bpy)_2(4,4'\text{-}(CO_2H)_2bpy)](PF_6)_2$ attached to the glass side of an $In_2O_3$:Sn electrode with $CH_3CN$ as the external solvent. The emission maximum occurred at 637 nm (15 700 cm$^{-1}$) and the full width at half-maximum (fwhm) was 1790 cm$^{-1}$. For the complex in acetonitrile solution, the emission maximum occurred at 680 nm with a fwhm of 1780 cm$^{-1}$. These values were obtained for surfaces with incomplete coverages. In a series of studies where the concentrations of Ru(II) in the derivatization solution was varied from $2.5 \times 10^{-6}$ to $3 \times 10^{-5}$ M, the emission maximum, with dichloromethane as the external solvent, varied from 644 to 674 nm. Under identical experimental conditions, the integrated emission intensity from these electrodes decreased by a factor of 1.6 as the degree of surface loading was increased to full coverage.

Emission decay kinetics for the excited state of $[Ru(bpy)_2(4,4'\text{-}(CO_2H)_2bpy)](PF_6)_2$ attached to the glass side of an $In_2O_3$:

(24) (a) Meyer, T. J. *Pure and Appl. Chem.* **1986**, *58*, 1193. (b) Juris, A.; Balzani, V.; Barigelletti, F.; Campagna, S.; Belser, P.; Von Zelewsky, A. *Coord. Chem. Rev.* **1988**, *84*, 85.

(25) (a) Lay, P. A.; Sasse, W. H. F. *Inorg. Chem.* **1984**, *23*, 4123. (b) Ferguson, J.; Mau, A. W.-H.; Sasse, W. H. F. *Chem. Phys. Lett.* **1979**, *68*, 21.

(26) (a) Brazdll, J. F.; Yeager, E. B. *J. Phys. Chem.* **1981**, *85*, 995. (b) Brazdll, J. F.; Yeager, E. B. *J. Phys. Chem.* **1981**, *85*, 1005.

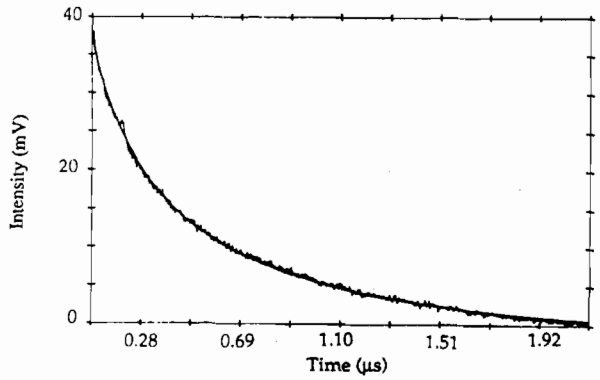


**Figure 11.** Emission decay (460 nm excitation wavelength monitored at 660 nm) for $[Ru(bpy)_2(4,4'-(CO_2H)_2bpy)](PF_6)_2$ attached to the glass side of an $In_2O_3$:Sn electrode by using a 45° front face geometry with $CH_2Cl_2$ as the external solvent. The overlaid, smooth curve is the fit of the data to eq 1 by using the parameters $k = 5.58 \times 10^6\ s^{-1}$ and $\beta = 0.506$.

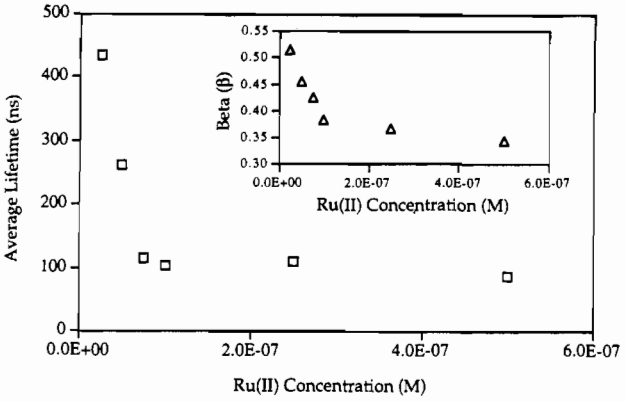


**Figure 12.** Dependence of $\langle\tau\rangle$ and $\beta$ as a function of $[Ru(bpy)_2(4,4'-(CO_2H)_2bpy)](PF_6)_2$ in the external acetonitrile derivatization solution. The emission data were acquired following 460-nm excitation monitored at 660 nm with dichloromethane as the external solvent. The quantities $\langle\tau\rangle$ and $\beta$ are defined in eqs 1 and 2.

Sn electrode (460-nm excitation) were nonexponential in air, cyclohexane, acetonitrile, and dichloromethane. The decays could be fit to the Williams–Watts (Kohlrausch) function in eq 1. A typical decay trace in $CH_2Cl_2$ and the kinetic fit of the data are shown in Figure 11. The average lifetime $\langle\tau\rangle$ for the surface-attached species with dichloromethane as the external solvent varied significantly from electrode to electrode, even when the same derivatization solution was employed. These variations could be as great as a factor of 10. In one study in which 12 electrodes were derivatized in an acetonitrile solution $5 \times 10^{-7}$ M in Ru(II), the average lifetimes varied from 54 to 259 ns. A measure of reproducibility was obtained in a series of studies where the surface coverage at a given electrode was increased by sequential soaking. It was observed that both $\langle\tau\rangle$ and $\beta$ from eqs 1 and 2 decreased with increasing surface coverage. In several series of experiments in which three to five identically-treated $In_2O_3$:Sn electrodes were successively derivatized in increasing concentrations of complex, the kinetic parameters $\langle\tau\rangle$ and $\beta$ were averaged, and their variation with surface coverage (measured at the metal oxide site by electrochemistry) is shown in Figure 12.

Control experiments demonstrated that >99.5% of the emission from the derivatized complexes orginates from the glass backing of the electrodes. In one experiment, two $In_2O_3$:Sn electrodes were derivatized in a $4 \times 10^{-6}$ M acetonitrile solution of the complex—but with opposite sides of the electrode coated with a thick layer of Type W Apiezon wax in cyclohexane. An emission was observed from the glass side of the electrode at 660 nm with $\langle\tau\rangle = 401$ ns with degassed acetonitrile in the external solution. Emission from the conducting side was barely perceptible with $\langle\tau\rangle < 5$ ns.

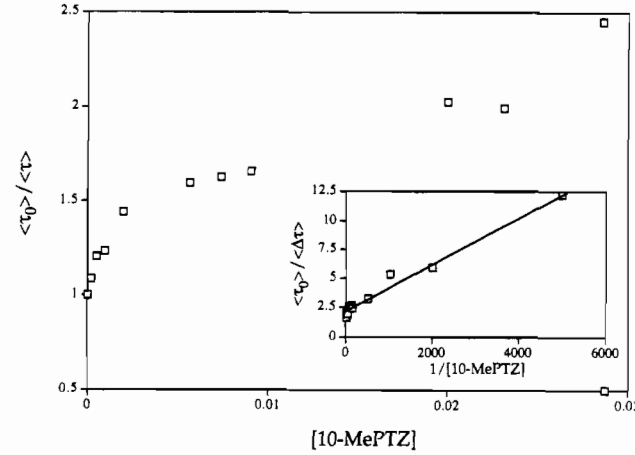


**Figure 13.** Influence on emission lifetime of 10-MePTZ on a glass slide derivatized with $[Ru(bpy)_2(4,4'-(CO_2H)_2bpy)](PF_6)_2$ with dichloromethane as the external solvent. Lifetimes were measured at 660 nm following 460-nm excitation. The inset depicts the data plotted according to eq 3b with $\langle\Delta\tau\rangle = \langle\tau_0\rangle - \langle\tau\rangle$. The abbreviations used are defined in the text.

Emission from $In_2O_3$:Sn electrodes derivatized by $[Ru(bpy)_2(4,4'-(CO_2H)_2bpy)](PF_6)_2$ was quenched upon addition of 10-methyl-10*H*-phenothiazine (10-MePTZ) to the external

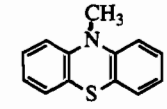


10 Me-PTZ

dichloromethane solution. In Figure 13 is depicted a Stern–Volmer plot obtained for lifetime quenching for a submonolayer-derivatized electrode with an unquenched average lifetime $\langle\tau_0\rangle = 550$ ns. The decrease in lifetime does not follow simple Stern–Volmer kinetics, and there was a residual emission with $\langle\tau\rangle \sim 190$ ns, which was never completely quenched. The kinetic treatment in eq 3 linearizes the data with the parameters: $f_i = 0.47$ and $K_{SVi} = 1070\ M^{-1}$. With this value and $\langle\tau_0\rangle = 598$ ns, $\langle k_q\rangle = 1.8 \times 10^9\ M^{-1}\ s^{-1}$ for the average quenching rate constant.

The effect of co-attached carboxylic acid quenchers on the derivatized slides was also investigated. A series of identically-treated ITO electrodes were derivatized in a $4 \times 10^{-6}$ M acetonitrile solution of $[Ru(bpy)_2(4,4'-(CO_2H)_2bpy)](PF_6)_2$ for 2.5 h, followed by derivatization in $5 \times 10^{-5}$ M solutions of the appropriate carboxylic acid quencher, PTZ-$CO_2H$, $[MV-CO_2H](PF_6)_2$, or $[Os(bpy)_2(4,4'-(CO_2H)_2bpy)](PF_6)_2$, for an additional hour. The control (unquenched) electrode exhibited an average lifetime of 120 ns. Emission decay from the electrode co-attached with PTZ-$CO_2H$ occurred with $\langle\tau\rangle = 30$ ns and with $MV^{2+}$-$CO_2H$, $\langle\tau\rangle = 20$ ns. The electrode co-attached with $[Os(bpy)_2(4,4'-(CO_2H)_2bpy)](PF_6)_2$ had no emission at 660 nm, but a new emission appeared at 810 nm, the emission maximum for the derivatized osmium complex, with $\langle\tau\rangle < 5$ ns. In a separate experiment in which the mole fractions of Ru(II) and Os(II) in the derivatization solution were varied at an overall concentration of $1 \times 10^{-4}$ M, the following values were obtained: $\chi_{Ru} = 1.0$; $\langle\tau\rangle_{660\ nm} = 313$ ns; $\chi_{Ru} = 0.6$, $\langle\tau\rangle_{660\ nm} = 116$ ns, $\langle\tau\rangle_{810\ nm} < 5$ ns; and $\chi_{Ru} = 0.0$, $\langle\tau\rangle_{810\ nm} < 5$ ns.

## Discussion

Our observations extend and reinforce the results of earlier studies on surface attachment to oxide electrodes and glass surfaces based on carboxylic acid functional groups.[4-7] They have also opened new directions based on extension of the surface chemistry to include a variety of organic and inorganic redox couples, a

complex that is a known oxidation catalyst in solution, and complex assemblies containing more than one type of redox site.

**Surface Binding and Resonance Raman.** One issue that we hoped to address was the nature of the interaction between the adsorbed molecules and the various surfaces. The resonance Raman technique provides a direct probe by allowing for the acquisition of high-quality vibrational data on surfaces where the number of sites is low. This technique has been successfully applied to a variety of adsorbed species at solid-gas interfaces,[25] $[Ru(bpy)_3]^{2+}$ on porous Vycor glass,[27] and bipyridyl complexes of $Ru^{II}$ on $TiO_2$.[28] For $[Ru(bpy)_3]^{2+}$ on porous Vycor, frequency shifts compared to $[Ru(bpy)_3]^{2+}$ in solution are insignificant although changes were observed in the relative intensities of the Raman bands.[27] From these observations, it was concluded that ground and excited state structures for $[Ru(bpy)_3]^{2+}$ either adsorbed or in solution were similar, but that there are structural differences in the excited state in the two media. The spectra of $[Ru(4,4'\text{-}(CO_2H)_2bpy)_3](PF_6)_2$ on $TiO_2$ and in solution are similar and it has been suggested that surface binding is by solvent-separated physisorption.[28]

Typically, seven relatively intense bands appear resonantly enhanced in Raman spectra of bpy complexes.[29] These are totally symmetrical framework modes. In $[Ru(bpy)_3]^{2+}$, the bpy modes that show the greatest enhancement are $\nu_7$ at 1489, $\nu_6$ at 1560, and $\nu_5$ at 1605 $cm^{-1}$ (the band designations are from ref 29b). In the mixed-ligand complexes, $[Ru(bpy)_2(4,4'\text{-}(CO_2H)_2bpy)]^{2+}$ and $[Ru(bpy)_2(4,4'\text{-}(CO_2Et)_2bpy)]^{2+}$, assignment of some of the framework modes for the substituted bpy ligand can be made by comparing their spectra with $[Ru(bpy)_3]^{2+}$. From Table 2, vibrations analogous to $\nu_7$, $\nu_6$ and $\nu_5$ for bpy appear at 1475, 1550, and 1615 $cm^{-1}$ for the diacid substituted ligand. The primed notation is used to distinguish these modes in Table 2. On the basis of comparisons with the spectra of $[Ru(4,4'\text{-}(CO_2H)_2bpy)_3]^{2+}$ and $[Ru(4,4'\text{-}(CO_2Et)_2bpy)_3]^{2+}$,[28] some of the remaining bands appear to be overlapped for the two types of ligands in the mixed-ligand complexes.

The band at 1550 $cm^{-1}$ that appears in the spectra of both the ester and the carboxylic acid derivatives (spectra B and C in Figure 5) shifts to 1540 $cm^{-1}$ for the carboxylato derivative. The band near 1730 $cm^{-1}$ for the ester or carboxylic acid derivatives can be assigned to $\nu$(C=O) of the substituted bpy ligand. This band appears for $[Ru(bpy)_2(4,4'\text{-}(CO_2Et)_2bpy)](PF_6)_2$ in $CH_2Cl_2$ as a band of medium intensity at 1730 $cm^{-1}$ and is also observed in the IR spectrum at 1730 $cm^{-1}$. For the carboxylic acid derivative, $\nu$(C=O) appears at 1725 $cm^{-1}$ in the IR and Raman, with low intensity in the latter spectrum (C). For the carboxylato derivative, there was no resonantly Raman band in the region 1700–1750 $cm^{-1}$, but a band of medium intensity at 1292 $cm^{-1}$ appeared which can be assigned to the coupled, symmetrical carbonyl stretch ($\nu_{sym}(CO_2^-)$). The coupled asymmetrical stretch ($\nu_{asym}(CO_2^-)$) appears at 1620 $cm^{-1}$ in the IR.[22,30]

The most obvious feature to emerge from comparisons between solution spectra and spectra on $SiO_2$ or $SnO_2$ is the absence of a peak assignable to $\nu$(C=O) between 1700 and 1750 $cm^{-1}$ for the complex attached to $SiO_2$. On $SnO_2$ or $TiO_2$, a resonantly enhanced peak of low intensity does appear near 1690 $cm^{-1}$ which can be assigned to $\nu$(C=O). On glass, a peak of medium intensity appears as a shoulder at 1305 $cm^{-1}$, which is likely $\nu_{sym}(CO_2^-)$ by comparison to the carboxylato derivative where $\nu_{sym}(CO_2^-)$ appears at 1292 $cm^{-1}$. This peak is not observed on $SnO_2$ or $TiO_2$. There are other similarities between the spectrum of the carboxylato derivative and the complex on $SiO_2$. The Raman peak at 1550 $cm^{-1}$ for the acid and ester complexes (1540 $cm^{-1}$ in the carboxylato derivative) appears at 1538 $cm^{-1}$ on $SiO_2$ and at 1544 $cm^{-1}$ on $SnO_2$ and $TiO_2$. A Raman peak of low intensity at 1374 $cm^{-1}$ gains intensity in both the carboxylato derivative and the complex on $SiO_2$.

**Chart 1**

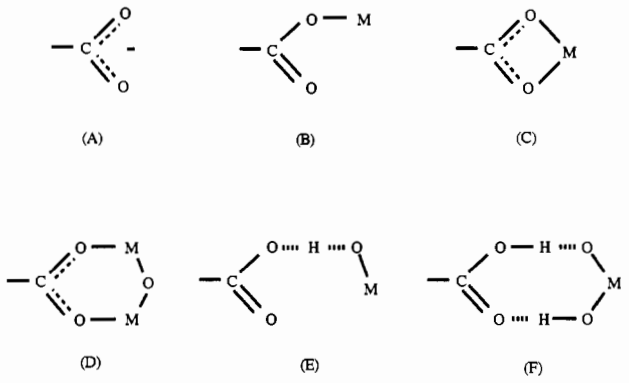


The frequency differences which exist between the complexes on the surfaces and in solution argue against a solvent separated adsorption to the surface. On $SiO_2$, $\nu_{sym}(CO_2^-)$ shifts to 1305 $cm^{-1}$ compared to 1292 in solution. Other changes occur in $\nu_6'$ which shifts from 1540 $cm^{-1}$ in solution to 1538 $cm^{-1}$ on $SiO_2$ and the Raman band at 1254 $cm^{-1}$ is shifted to 1249 $cm^{-1}$. Changes of this magnitude are also evident for $[Ru(bpy)_2(4,4'\text{-}(CO_2H)_2bpy)](PF_6)_2$ on $SnO_2$ or $TiO_2$ compared to the ester derivative in solution. In this case $\nu$(C=O) shifts from 1730 $cm^{-1}$ in solution for the ester complex to 1691 $cm^{-1}$ on $SnO_2$. Also, there is a shift in $\nu_6'$ to 1544 $cm^{-1}$ on $SnO_2$ compared to 1550 $cm^{-1}$ for the ester derivative.

A number of possibilities remain for the nature of the interaction(s) between the acid derivatives and the surfaces. They include physical adsorption (perhaps via hydrogen bonding) or chemical bond formation to the surface by unidentate, chelating, or bridging modes of attachment. These are illustrated in Chart 1, where M is a surface ion or atom (Si, Sn, or Ti). A variety of hydrogen-bonding structures could be drawn involving one or both of the carboxylato groups, two are illustrated in the chart.

The similarities between the spectra on $SnO_2$ and $TiO_2$ and the ester derivative in solution point to chemical bonding and ester formation to the surface and **B** in Chart 1 or to any one of a number of H-bonding structures such as **E** or **F**. If H-bonding is important, there must be a relatively stable structure at the surface. The spectrum on $SiO_2$ is nearly identical to the spectrum of the carboxylato derivative, which points to either chelate, **C** in Chart 1, or bridge bonding (**D**). There may be an additional, different mode of binding to $SiO_2$ as evidenced by the appearance of a weak band at 1550 $cm^{-1}$ in the Raman spectrum and at 1720 $cm^{-1}$ in the IR. The appearance of these bands points to a second, minority mode of binding on $SiO_2$ based on structure **B** and ester or H-bond formation.

Deacon and Phillips have drawn general conclusions regarding carboxylato binding to metal ions by examining vibrational spectroscopy and X-ray crystallographic data for a series of acetates and trifluoroacetates.[31] In this approach, the positions and differences between carboxylato frequencies in complexes and ionic salts ($\Delta$) are compared. As a unidentate ligand, carboxylato loses the equivalence of the two carbon-oxygen bonds and the peak near 1600 $cm^{-1}$ in the free ion shifts to higher energy. The magnitudes of $\Delta$ for $\nu_{asym}(CO_2^-) - \nu_{sym}(CO_2^-)$ or $\nu$(C=O) $- \nu$(C—O) are greater for ester-type linkages (structure **B**) than for ionic carboxylates. The data for $[Ru(bpy)_2(4,4'\text{-}(CO_2H)_2$-

(27) Shi, W.; Wolfgang, S.; Strekas, T. C.; Gafney, H. D. *J. Phys. Chem.* **1985**, *89*, 974.
(28) Umapathy, S.; Cartner, A. M.; Parker, A. W.; Hester, R. E. *J. Phys. Chem.* **1990**, *94*, 8880 and references therein.
(29) (a) Dallinger, R. F.; Woodruff, W. H. *J. Am. Chem. Soc.* **1979**, *101*, 1355. (b) Strommen, D. P.; Mallick, P. K.; Danzer, G. D.; Lumpkin, R. S.; Kincaid, J. R. *J. Phys. Chem.* **1990**, *94*, 1357.
(30) Nakamoto, K. *Infrared and Raman Spectra of Inorganic and Coordination Compounds*, 4th ed.; John Wiley and Sons, Inc.: New York, 1986. See also ref 22 and references therein.
(31) Deacon, G. B.; Phillips, R. J. *Coord. Chem. Rev.* **1980**, *33*, 227.

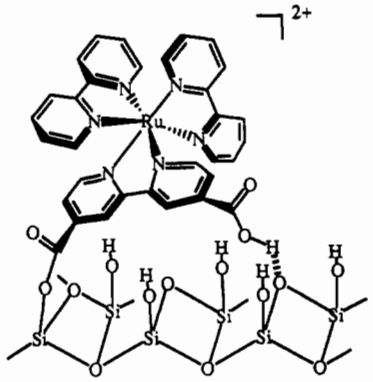

**Figure 14.** Schematic representation of the proposed single ester linkage and H-bonding of $[Ru(bpy)_2(4,4'\text{-}(CO_2H)_2bpy)](PF_6)_2$ with the surface of a $SnO_2$:Sb electrode based on *ab initio* calculations. See text for details.

bpy)]$(PF_6)_2$ bound to $TiO_2$ and $SnO_2$ are consistent with this type of attachment.

Both symmetrical chelation (structure **C**) and bridging carboxylates (**D**) maintain the equivalence of the two CO bonds found in the free ion (**A**). The chelating mode would result in a smaller O–C–O angle than the bridging mode. Values of $\Delta$ less than those observed for ionic salts are indicative of the chelating or bridging structure. Typically, $\Delta$ values for chelating structures are much less than for ionic salts and are greater or comparable for bridging structures.

From the Raman and IR data, $\Delta = 328\ cm^{-1}$ for the carboxylato derivative and $\Delta = 335\ cm^{-1}$ on $SiO_2$ for the majority sites. On the basis of this comparison and general conclusions regarding carboxylato binding, the bridging mode, structure **D** in Chart 1, is suggested for the majority sites. This is a somewhat equivocal conclusion, less certain than the conclusion of an ester link or H-bonding on $SnO_2$ and $TiO_2$.

The suggestion has been made in the literature that binding to the surfaces of metal oxides, at least for cases like $[Ru(tpy)(4,4'\text{-}(CO_2H)_2bpy)(H_2O)](PF_6)_2$, where there is a replaceable water molecule, may occur via M–O–Ru bond formation.[28] This is clearly *not* the case for the tpy complex. This point is demonstrated by the appearance of the expected pH dependence for the Ru(III/II) couple associated with loss of a proton in the more acidic, Ru(III) oxidation state.[12] The acid–base properties of the couple may be retained, but the surface has a profound effect on lability of the bound aqua ligand. The decrease in exchange rate of $CH_3CN$ for $H_2O$ by >250 on the surface is dramatic. It may be a binding effect arising because the $Ru\text{–}OH_2^{2+}$ group is held close to the surface.

It is clear that a single carboxylato group, and by inference, a single ester or H-bonding network to the surface, is sufficient to create stable surface structures. It is not clear from the resonance Raman data as to whether one or both of the carboxylato groups of $[Ru(bpy)_2(4,4'\text{-}(CO_2H)_2bpy)](PF_6)_2$ are bound. Resonance Raman can not distinguish between the two possibilities because differences in band energies between surface bound carboxylato and free acid are negligible. The evidence for two modes of binding on glass could reflect the fact that at least some of the sites are singly bound to the surface with the second "ester" type site being an unbound carboxylic acid group or H-bonded to the surface.

We have investigated surface binding by using molecular modelling calculations.[32] The results of these calculations suggest that ester bond formation to the surface by both carboxylic acid groups on a single bpy is not favorable due to van der Waals repulsions with the H-atoms on the surface hydroxyl and with the Si–O–Si $\mu$-oxo groups. Hydrogen-bonding to the surface for the second $-CO_2H$ group is possible, as shown in Figure 14, via O–H··O bonding to a surface O with H··O at 3.2 Å, or by surface hydroxyl hydrogen-bonding to the carbonyl.

If the conclusion of single ester bond formation is correct, the surface attachment reaction is as shown in eq 7 for $[Ru(bpy)_2(4,4'\text{-}(CO_2H)_2bpy)](PF_6)_2$ with $SnO_2$:Sb as the substrate. There is evidence for retention of the $PF_6^-$ anions from XPS measurements, with 1s F and 2p P peaks occurring with binding energies of 136.6 and 686.8 eV, respectively.[33]

$$\text{Sn–OH} + [Ru(bpy)_2(4,4'\text{-}(CO_2H)_2bpy)](PF_6)_2 \longrightarrow \text{Sn–O–C(O)–4'-(CO}_2\text{H)bpy)Ru(bpy)}_2](PF_6)_2 + H_2O \quad (7)$$

With this model, the Langmuir analysis (which assumes a fixed number of equivalent, non-interacting sites)[23] of the surface binding data yields a constant $K$, which is characteristic of single ester formation and is equal in magnitude for both metal oxides, $K\ (CH_2Cl_2, 293\ K) = (8 \pm 6) \times 10^4\ M^{-1}$. The indifference of $K$ to added electrolyte in the derivatizing solutions is further evidence that electrostatic binding is not the mode of binding to the surface. Values of $K$ in the same range have been measured by Grätzel and coworkers for trinuclear, cyano-bridged ruthenium(II) carboxylatobipyridine complexes.[34]

Because of the roughened character of the metal oxide surfaces, Figure 2, it was surmised that there could be less than actual monolayer surface coverages on "fully derivatized" electrodes with the extent of surface coverage dictated, in part, by the availability of active surface hydroxyl goups rather than by close contact repulsion between neighbors. However, silanol numbers (the number of surface OH groups/nm²) for $SiO_2$, $Al_2O_3$ (which is structurally analogous to $In_2O_3$), and $TiO_2$ (analogous to $SnO_2$) are 4.6, 12–13, and 7, respectively at 298 K.[35a,b] Assuming a close-packed structure for the Ru complex, only 2.2 OH groups/nm² would be covered, lending support to the notion that surface binding is not surface hydroxyl limited.[35c] This result would imply that surface coverages on the metal oxide and glass sides of the electrodes should be similar, since in both cases, surface binding is limited by the size of the Ru complex. On the glass side of the electrodes, emission measurements provide evidence for neighboring excited state–ground state interactions, which increase as surface coverage increases (see below), and excited state quenching by electron or energy transfer to coattached quenchers is observed.

The observation of lower than monolayer coverages for the smaller organics may be due to their relatively flexible links to the surface which impart an ability to bend over and lie longitudinally on the metal oxide surfaces. "Limiting coverages" of as much as 10× greater for $[Ru(tpy)(4,4'\text{-}(CO_2H)_2bpy)(H_2O)](PF_6)_2$ need to be explored in more detail. Multilayer coverages of this kind almost demand extended structures based on intermolecular H-bonding.

**Electrochemistry and Absorption and Emission Spectra.** The electrochemical properties of $[Ru(bpy)_2(4,4'\text{-}(CO_2H)_2bpy)]$-

(32) The molecular modeling was performed by using a 3-21G* *ab initio* calculation. The calculation included full geometry optimization of both the complex and the $SiO_2$ surface with ~1.79 Å Si–O and ~0.95 Å O–H bond lengths. The calculation was based on a $SiO_2$ particle of radius ~18 Å. A 360° pivot around the Si–OCO– axis was also employed in the calculations.

(33) van Attekum, P. M. Th. M.; van der Velden, J. W. A.; Trooster, J. M. *Inorg. Chem.* **1980**, *19*, 701.

(34) Nazeeruddin, M. K.; Liska, P.; Moser, J.; Vlachopoulos, N.; Grätzel, M. *Helv. Chim. Acta* **1990**, *73*, 1788.

(35) (a) Iler, R. K. *The Chemistry of Silica*; Wiley & Sons, Inc.: New York, 1979; pp 633–636. (b) Johnston, L. J. In *Photochemistry in Organized & Constrained Media*; Ramamurthy, V., Ed.; VCH Publishers: New York, 1991; Chapter 8. (c) This calculation is based on the average value of 4.6 OH groups/nm² found in ref 35a.

$(PF_6)_2$ in solution have been described previously.[25] On the $SnO_2$:Sb or $In_2O_3$:Sn electrodes, the potential of the attached couple was ~60 mV less than $E_{1/2}$ for $[Ru(bpy)_2(4,4'\text{-}(CO_2H)_2bpy)]^{2+}$ and >140 mV more positive than $E_{p,a}$ for $[Ru(bpy)_2(4,4'\text{-}(CO_2^-)_2\text{-}bpy)]$. The shift to a more positive potential compared to $[Ru(bpy)_2(4,4'\text{-}(CO_2^-)_2bpy)]$ is also consistent with surface binding by ester formation. This is a substituent effect since the ester groups are electron withdrawing which increases the extent of $d\pi$ Ru(II)–$\pi^*(4,4'\text{-}(X)_2bpy)$ mixing. The substituent effect appears in the spectroscopic data in Table 1, although more ambiguously.[36] In $CH_3CN$, there is an decrease in emission energy from 639 nm for $[Ru(bpy)_2(4,4'\text{-}(CO_2^-)_2bpy)]$ to 655 nm on the surface, although the shift is greater to the diester (687 nm) or acid (680 nm) derivatives in $CH_3CN$. That there would be shifts between the ester-derivatized and surface-bound emitters is not surprising; MLCT emission energies and lifetimes are known to be medium dependent.[24a,37]

Evidence for surface attachment is reinforced by the appearance of stable voltammograms such as those shown in Figure 3. Only background charging currents are observed over this potential window when underivatized electrodes were placed in the same solution. The reductive and oxidative currents are directly proportional to the scan rate, and the voltammograms are not affected by stirring the electrolyte solution, consistent with surface attachment.[21] The appearance of the dark redox chemistry is consistent with a description of the doped metal oxides being classified as degenerate semiconductors.[38]

The full-width-at-half-maxima ($E_{fwhm}$) of the voltammetric waves (~200 mV) was considerably larger than the expected 90.6 mV.[21] This observation is consistent with repulsive interactions between sites in the charged monolayers, slow electron transfer, or a dispersion of sites having different $E_{1/2}$ values.[21] The nonzero peak to peak splitting observed for all surface attached couples is consistent with either slow interfacial electron transfer or uncompensated resistance. We believe slow electron transfer makes a major contribution since the peak-to-peak splitting is independent of the area of the working or counter electrodes and the electrolyte concentration. Qualitatively, peak-to-peak splitting does decrease with decreased scan rate. Additional evidence on this point comes from the experiments on the "roughened" $SnO_2$:Sb electrodes. On those surfaces, there is evidence for two distinct sites, one of which undergoes slow heterogeneous electron transfer.

The redox properties of the individual couples on mixed surfaces of $[Ru(bpy)_2(4,4'\text{-}(CO_2H)_2bpy)](PF_6)_2$ with $[Os(bpy)_2(4,4'\text{-}(CO_2H)_2bpy)](PF_6)_2$ or of PTZ-$CO_2H$ with $[MV\text{-}CO_2H](PF_6)_2$ are retained on $In_2O_3$:Sn. The $E_{1/2}$'s for these couples are relatively unperturbed compared to surfaces containing each one singly. The importance of these experiments is that they demonstrate that lateral molecular assemblies containing mixed components can be formed on the metal oxide surfaces.

**Photophysical and Photochemical Properties.** On the oxide coated glass substrates, emission comes from surface bound species on the glass backing. It is almost completely quenched (> 99.5%) on the semiconductor side, with a decrease in lifetime for $[Ru(bpy)_2(4,4'\text{-}(CO_2H)_2bpy)](PF_6)_2$ from 1.4 μs in $CH_2Cl_2$ to <5 ns on ITO. There are some unusual features in the excited state properties of the Ru complex bound to glass. Excited state decay curves were nonexponential in organic solvents, in air, and in vacuo, Figure 11. These decays could be satisfactorily fit to the Williams–Watts (Kohlrausch) function, which assumes that there is a distribution of excited state lifetimes. Nonexponential luminescence decay for related excited states has been observed previously on a soluble polystyrene polymer derivatized with added ruthenium polypyridyl complexes[39] and in styryl-based polymeric films.[40] In the films, the nonexponential behavior has a number of origins, including multiple sites, excited state–ground state electronic coupling between adjacent sites, and the relatively slow relaxation of the film environment.[41] The latter effect, which is manifested in time-dependent emission spectra, couples structural relaxation in the films with excited state decay and creates a time-dependent distribution of excited state lifetimes.

There is direct evidence for interactions between sites on the glass surfaces. As the surface coverage of the emitter increases, the emission maximum shifts to lower energies (644–674 nm), the average lifetime decreases, and the degree of nonexponentiality ($\beta$) increases (Figure 12). These results are consistent with interacting surface sites at higher surface loadings. As found in the film study mentioned above, excited-ground state electronic interactions may stabilize the excited state, leading to a decrease in emission energy. This would provide an effective quenching mechanism on the derivatized surface. Nonradiative lifetimes of MLCT excited states are known to be sensitive to the excited to ground state energy gap,[24a] and the mechanism of quenching may simply be the decrease in the excited state energy caused by the interaction. In contrast to the film results,[40] time-resolved emission measurements reveal that there is no time dependence at our earliest observation time (~5 ns). By inference, the changes in local structure induced by the excitation are rapid, at least compared to the styryl-based films.

Even at extremely low surface loadings, the decay kinetics were significantly nonexponential, Figure 12. These results imply the existence of other effects on $\langle\tau\rangle$ in addition to excited state–ground state interactions. One possibility is the presence of different binding sites at the surface (ester formation, H-bonding), which have different lifetimes. These sites may differ either chemically or physically in their location on the surface. The coexistence of H-bonding or ester-type and carboxylato-type linkages, implied by the surface Raman data, could be a contributing factor to a surface containing multiple sites.

The evidence for surface sites in reasonably close contact includes the observation of emission quenching on surfaces containing both the chromophore and an attached quencher. This includes both reductive and oxidative electron transfer, the former on surfaces containing $[Ru(bpy)_2(4,4'\text{-}(CO_2H)_2bpy)](PF_6)_2$ and PTZ-$CO_2H$ and the latter or surfaces containing the complex and $[MV\text{-}CO_2H](PF_6)_2$. Excited state quenching of $[Ru(bpy)_3]^{2+*}$ by these quenchers is well-established in solution.[42] When $[Os(bpy)_2(4,4'\text{-}(CO_2H)_2bpy)](PF_6)_2$ was co-attached to glass, energy transfer quenching was observed. The 660 nm emission of the Ru complex disappeared,[43,44] concomitant with the appearance of the short-lived 810 nm emission from Os. Electron or energy transfer in all three cases is facile with $\langle\tau\rangle < 5$ ns ($k_q > 2 \times 10^8$ s$^{-1}$) for energy transfer. From the $\langle\tau\rangle$ value for reductive quenching by PTZ-$CO_2H$, $\langle\tau\rangle \sim 30$ ns, $k \sim 3 \times 10^7$ s$^{-1}$, and for oxidative quenching by $[MV\text{-}CO_2H](PF_6)_2$, $\langle\tau\rangle \sim 20$ ns, $k \sim 5 \times 10^7$ s$^{-1}$. The three surface-based quenching processes are illustrated schematically in Scheme 1.

The experiments with 10-MePTZ in the external solution demonstrate that external quenching can occur as well. Lifetime quenching as a function of added 10-MePTZ did not follow Stern–

(36) Lever, A. B. P. *Inorg. Chem.* **1990**, *29*, 127.
(37) Lees, A. J. *Chem. Rev.* **1987**, *87*, 711.
(38) Morrison, S. R. *Electrochemistry at Semiconductor and Oxidized Metal Electrodes*; Plenum: London, 1980.
(39) Baxter, S. M.; Jones, W. E., Jr.; Danielson, E.; Worl, L.; Strouse, G.; Younathan, J.; Meyer, T. J. *Coord. Chem. Rev.* **1991**, *111*, 47.
(40) Surridge, N. A.; McClananhan, S. F.; Hupp, J. T.; Danielson, E.; Gould, S.; Meyer, T. J. *J. Phys. Chem.* **1989**, *93*, 294.
(41) Gardner, J. R.; Worl, L. A.; Gould, S.; Guadalupe, A.; Sullivan, B. P.; Caspar, J. V.; Meyer, T. J. Unpublished results.
(42) Hoffman, M. Z.; Bolletta, F.; Moggi, L.; Hug, G. L. *J. Phys. Ref. Data* **1989**, *18*, 219.
(43) The emission spectrum was fit by using a standard, one-mode Franck–Condon analysis; note eq 5 in ref 44, with $E_0 = 15\,700$ cm$^{-1}$, $S_M = 1.06$, $\hbar\omega_M = 1300$ cm$^{-1}$, and $\Delta\nu_{0,1/2} = 1790$ cm$^{-1}$.
(44) Chen, P.; Duesing, R.; Graff, D. K.; Meyer, T. J. *J. Phys. Chem.* **1991**, *95*, 5850.

**Scheme 1**

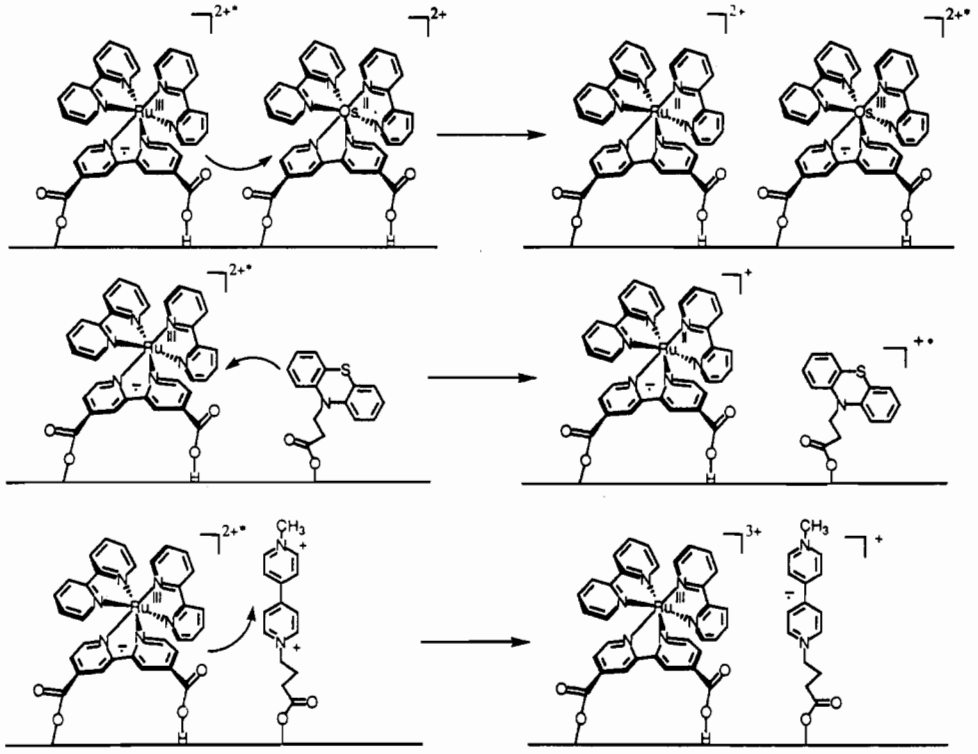

Volmer kinetics, but exhibited a more complex behavior reminiscent of quenching of $Ru^{II*}$ derivatized in chlorosulfonated polystyrene films.[40] It was found in the earlier study that the data could be fit to a model developed by Lehrer[17] which describes the quenching of protein-bound fluorophors by solution quenchers. The model assumes a distribution of sites on the protein backbone, some of which are accessible to solution quenchers while others are not. As shown in the inset of Figure 13, the linear correlation between $\langle\tau_0\rangle/\langle\Delta\tau\rangle$ and $[10\text{-MePTZ}]^{-1}$ predicted by the Lehrer treatment is observed for 10-MePTZ as the quencher in dichloromethane. On the basis of this analysis, the fraction of sites accessible to the quencher is ~0.47. These results point to the presence of at least two types of surface bound sites. One site is quenched by 10-MePTZ with a rate constant of $1.8 \times 10^9$ $M^{-1}$ $s^{-1}$, which is near the diffusion-controlled limit. The other site is not quenched. These results support the suggestion, raised in the photophysical measurements, that there are multiple sites on the surface. The surface structural basis for the sites not quenched by 10-MePTZ is not obvious, especially given the observation of nearly complete reductive quenching on surfaces containing co-attached $[Ru(bpy)_2(4,4'\text{-}(CO_2H)_2bpy)](PF_6)_2$ and PTZ-$CO_2H$. There may be some penetration within the surface layers and microchannel incursion to give sites which are not accessible to diffusion by 10-MePTZ on short timescales.

The fact that lateral electron and energy transfer can occur across the surfaces containing $[Ru(bpy)_2(4,4'\text{-}(CO_2H)_2bpy)](PF_6)_2$ bound to $SiO_2$ represents a major finding. An eventual goal is to combine attachment of monolayer molecular assemblies with lateral spatial control in order to explore long-range electron and energy transfer and the photoproduction of spatially-isolated oxidants and reductants.

**Acknowledgment.** This work was supported by the U.S. Army Research Office Grant No. DAAL03-88-K-0192 (to T.J.M.). C.A.B. was supported by Grant No. CRG 920184 from NATO.